Model learning of the tire–road friction slip dependency under standard driving conditions

Vincent Mussot, Guillaume Mercère, Thibault Dairay, Vincent Arvis, Jérémy Vayssettes

Model learning of the tire-road friction slip dependency under standard driving conditions

Vincent Mussot[a, b], Guillaume Mercère[b, 1], Thibault Dairay[a], Vincent Arvis[a] and Jérémy Vayssettes[a]

[a] *Manufacture Française des Pneumatiques Michelin, Clermont-Ferrand, France*
[b] *Laboratoire d'Automatique et d'Informatique pour les Systèmes, Poitiers University, Poitiers, France*

Abstract

The maximum tire-road friction coefficient is a quantity allowing to increase significantly the performance of the driver-assistance systems. Unfortunately, this value is particularly difficult to estimate under standard driving conditions. Therefore, this paper focuses on a parametric method based on Monte-Carlo Markov chain techniques to determine it accurately. Our solution combines the advantages of both a maximum likelihood method and an adaptive Metropolis algorithm to determine the tire-road friction coefficient. This approach requires friction measurements and a tire model representing the friction as a function of the slip ratio. After describing the theoretical aspects of the method, this paper focuses on its practical implementation. Several results obtained from both simulated data and real data are given to demonstrate the efficiency of the approach.

Keywords: tire-road friction estimation, parametric model learning, maximum likelihood method, MCMC estimation

1. Introduction

Because traffic accidents are responsible for a huge number of deaths every year all over the world, the passenger's safety is one of the priority for vehicle manufacturers [1]. In order to ensure this safety, passenger vehicles are nowadays equipped with control chassis systems such as the anti-lock braking system (ABS) or the electronic stability programs (ESP) [2]. These tools act on vehicle inputs to correct the vehicle trajectory or to prevent the wheels from locking up in dangerous situations. These dangerous situations often appear when the car is exposed to severe external conditions such as slippery roads or sudden avoidance manoeuvres at high speed. With the rise of autonomous vehicles and all the requirements necessary to create a vehicle that should drive itself without the intervention of a human driver, the driver assistance systems, commonly called Advanced Driver Assistance Systems (ADAS) [3], are particularly studied nowadays[4]. In the case of autonomous vehicles, ADAS should not only have corrective actions but also preventive ones in order to ensure the traffic fluidity. One of the path considered in the literature to develop these future ADAS goes through the acquisition of essential information influencing the vehicle behavior [5]. Among the information which

[1] CONTACT G. Mercère. Email: guillaume.mercere@univ-poitiers.fr

could improve the ADAS, the maximum friction coefficient [6] also called the grip potential or maximum tire-road friction coefficient [7] is paramount. The maximum friction coefficient represents the maximum effort a tire can transmit to the ground [8] before it begins to slip on the road. This grip potential mainly depends on three different components, *(i)* the tire (model, dimensions, pressure, wear), *(ii)* the ground (type of covering, state of the road) and *(iii)* the presence of a third element at the interface between the tire and the road such as snow, water or dust [9]. Furthermore, knowledge of the grip potential value turns out to be advantageous in various situations such as during emergency manoeuvres because it allows the ADAS to brake with the optimal brake pressure and thus to reduce the stopping distance or to anticipate the right trajectory. In addition to these cases, the tire-road friction coefficient can also be used to detect the low grip area and thus reveals problems such as worn roads, poor rainwater drainage or need for snow removal [10].

Several studies have been carried out to estimate the maximum friction coefficient [3, 8, 11, 12]. They can be separated into two main categories. In the first class of solutions, the tire-road friction coefficient is estimated directly by using dedicated (thus costly) sensors. Convincing results were obtained with this approach [11]. However, ADAS are intended to be used on production vehicles where the use of expensive sensors is an obstacle [13]. Therefore, cost-effective methods using exclusively the sensors already used on production cars should be considered. These methods are mainly part of the second category usually called the model-based methods. As the name suggests, model-based methods use models combined with measurements to make predictions of the tire-road friction coefficient. Among the model-based methods, we can distinguish the nonparametric methods, which use essentially black-box models [14], from the parametric methods which include a physical model representing the tire behavior. For example, in [15], the author employs Gaussian processes to learn the friction curve from production car sensors. Thus, this method enables to determine not only the grip potential but also the entire friction curve as a function of the slip ratio. However, this method requires, like many other methods, high-friction data points to give reliable results. Indeed, according to [16], both parametric and nonparametric model-based methods require excitations providing a friction consumption level between 0.3 and 0.8 to be able to provide a reliable estimate of this grip potential. Unfortunately, under normal driving conditions, the measurements available do not exceed generally a friction of 0.3 (see Figure 1). This corresponds to a lower excitation level than the one required by most of the model-based methods. Thus, the main difficulty for estimating the grip potential lies in the fact that only low friction measurements are accessible during normal driving conditions.

Nevertheless, the literature provides some methods delivering interesting results with a low excitation level. One of them is a parametric model-based method introduced by Singh and Taheri in [10] where the grip potential is estimated by combining nonlinear least squares (NLLS) parameter estimation of the Brush model [17] and the frequency response of an accelerometer located in the tire. As shown in [10], this NLLS solution performs well once the friction measurements available are greater than 0.6 which is incompatible with low-excitation level. Therefore, in order to estimate the grip potential during free rolling phase (where the excitation is low), the authors propose to add a characterization of the road surface friction level by

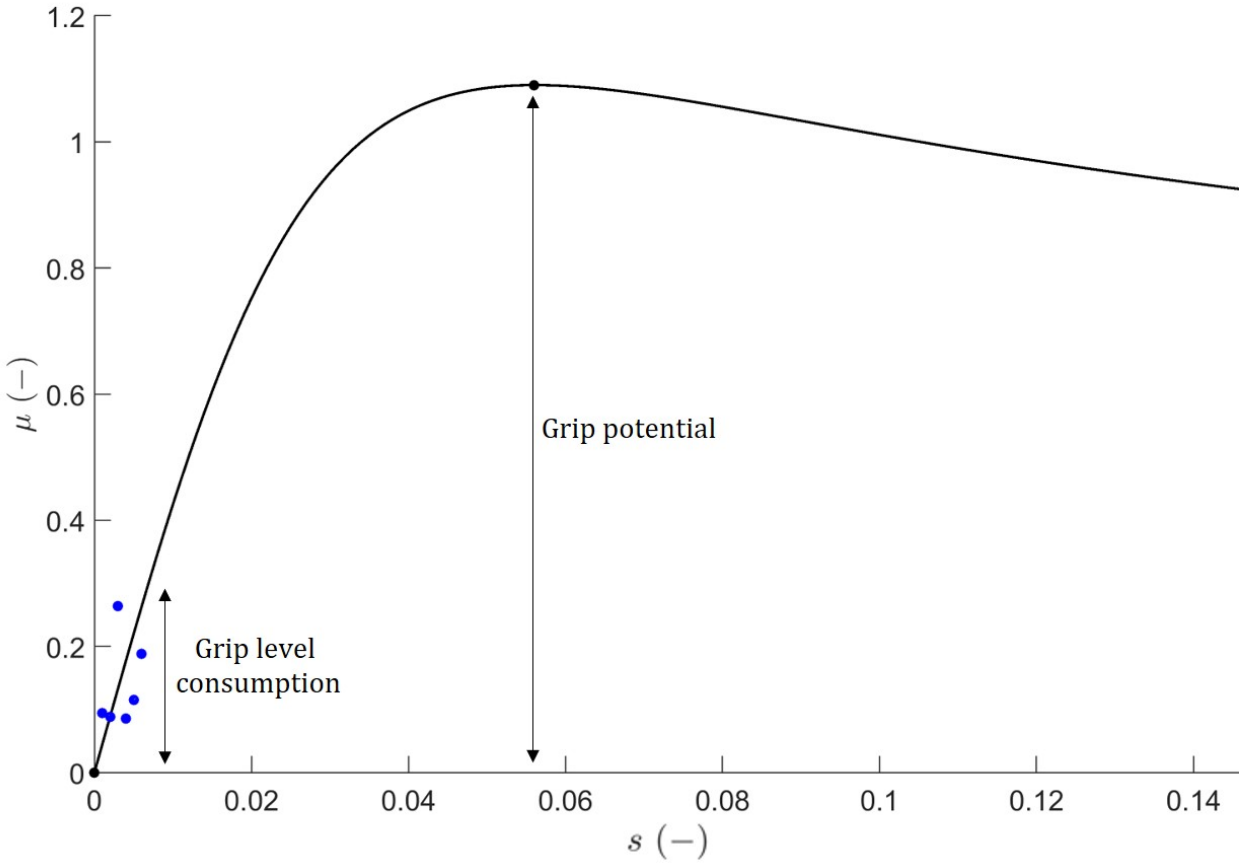

Figure 1: Example of tire friction curve. The blue points are the data points accessible under standard driving conditions.

studying the frequency response of an accelerometer located in the tire. This way, they can distinguish the low-friction road portions from the high-friction ones. However, this method requires instrumented tire with an accelerometer and thus cannot be used with standard tires mounted on production vehicle.

Another method providing interesting results with low-friction measurements is the slip-slope method introduced by Gustafsson in [18]. This method is based on the assumption that the slip-slope (defined by the initial slope of the friction curve) depends on the grip potential. Thus, under this assumption, if the slip-slope is estimated, which is possible with the measurements available, the grip potential can be determined. The slip-slope method has been particularly discussed and the literature contains contradictory conclusions [3]. For some authors, the method is applicable with small friction measurements (lower than 0.3) [12]. For others, it requires higher friction (around 0.4 at least) and additional investigations to conclude on the validity of the method [3]. In addition, as pointed out by Gustafsson in [18], the slip-slope depends on several factors such as the tire inflation pressure, the tire temperature or the tire wear. Therefore, the method is effective only if all these factors are known. Thus, this method necessitates a calibration to be effective. This point is

however not the main issue of this method. The main problem of the slip-slope method is the fundamental assumption of a link between the slip slope and the grip potential [3]. As mentioned in [18], this link has not been proven theoretically yet. Tests to establish the existence of this link are performed in [19] but the authors conclude that a link between the slope and the tire-road friction coefficient cannot be confirmed. Hence the slip-slope method needs more examinations to verify if it can provide a reliable estimate of the grip potential in all situations. For all the above mentioned reasons, another method is suggested here to estimate the maximum friction coefficient.

As mentioned earlier, friction measurements can come from real sensors while standard driving conditions must be accounted for. For these reasons, these measurements are corrupted by noise and are almost always lower than 0.3. These constraints on the measurements can make difficult the use of nonparametric methods which are particularly efficient in interpolation, but might be less appropriate to estimate points far from the measurement area as it is the case here. Hence, a parametric model-based approach will be considered hereafter to estimate the tire friction potential. The method suggested in this paper is a tire curve fitting method based on a Maximum Likelihood (ML) method and an adaptive Monte-Carlo Markov Chain (MCMC) method [20], respectively. The MCMC method is suggested because it has the advantage to work well with few points and enables the user to take into consideration the noise properties effectively [14]. This method requires the use of a tire model which should represent the tire behavior in various situations accurately. One tire model fulfilling these conditions is the Pacejka's magic formula tire model [21]. This model is commonly used by tire manufacturers because it is a parsimonious model which represents accurately the tire behavior. Therefore, the approach suggested in this paper consists in estimating the unknown parameters of the Pacejka's model by initializing an MCMC method with ML estimates.

The rest of the paper is organized as follows. Section 2 is dedicated to the description of the problem and the notations used in this paper. Section 3 describes the method used herein to estimate the tire-road friction coefficient and underlines the different settings necessary to maximize the method performance. Section 4 presents the results obtained when the method is tested with simulated data and real data, respectively. Finally, Section 5 concludes this paper.

2. Problem formulation and notations

In this paper, we aim at determining the maximum of the tire-road friction from noisy and short data sets acquired with standard sensor signals. This maximum value, called in the literature the tire friction potential or the grip potential [16], is the maximum force a tire can generate before sliding. More precisely, when only longitudinal dynamics is considered [2], the tire friction μ is defined as follows [22]

$$\mu = \frac{F_x}{F_z}, \tag{1}$$

[2]Notice that, most of the time, a car drives straightforward [12].

and thus, the grip potential is

$$\mu_{\max} = \max\left(\frac{F_x}{F_z}\right), \tag{2}$$

where F_x and F_z are the longitudinal tire force and the tire normal load, respectively.

As shown, *e.g.*, in [23], the friction μ, and by extension the grip potential $\mu_{\max}$, is impacted by several quantities such as the tire inflation pressure, the tire temperature, the tire load or the tire tread depth to name a few. Among all these quantities, the slip ratio s defined by (see Table 1 for the definition of ω, R_r and v, respectively)

$$s = \frac{\omega R_r - v}{\max(\omega R_r, v)}, \tag{3}$$

plays a central role [24]. The basic idea of the solution developed in this paper is to determine the friction dependency in the slip ratio s with a (parametric) model

$$\mu = f(s), \tag{4}$$

and to compute its maximum straightforwardly.

Table 1: Signals and parameters used for defining the slip ratio.

Symbol	Definition	Units
ω	wheel speed	rad/s
R_r	wheel rolling radius	m
v	vehicle speed	m/s

Figure 2 illustrates standard but significant characteristics of this link between the tire friction μ and the slip ratio s. Such curves clearly show that the mapping $\mu = f(s)$ is a nonlinear function having a sharp initial slop, a maximum, then a gentle decrease with larger values of s. Besides, the different friction curves indicate that μ and thus μ_{max} depend of the road characteristics as well. For obvious practical reasons, it is essential that the model learning strategy introduced hereafter gives access to $\mu_{\max}$ accurately during "standard" driving conditions, *i.e.*, when only low values of μ (lower than 0.3) and s are observed. Said differently, the solutions developed in this paper to determine the grip potential $\mu_{\max}$ accurately must estimate this unknown mapping $\mu = f(s)$ from

- data sets acquired for low values of s, *i.e.*, far from the ones corresponding to the tire friction potential,
- real measurements acquired with standard sensors, *i.e.*, from noisy data sets.

In order to reach this goal, a data driven curve fitting, also named model learning solution, is suggested hereafter.

In addition to the aforementioned noisy data, the second ingredient of our model learning strategy is the choice of the mapping $f(\bullet)$. Different model structures have been suggested in the literature [21, 25, 26, 17, 27].

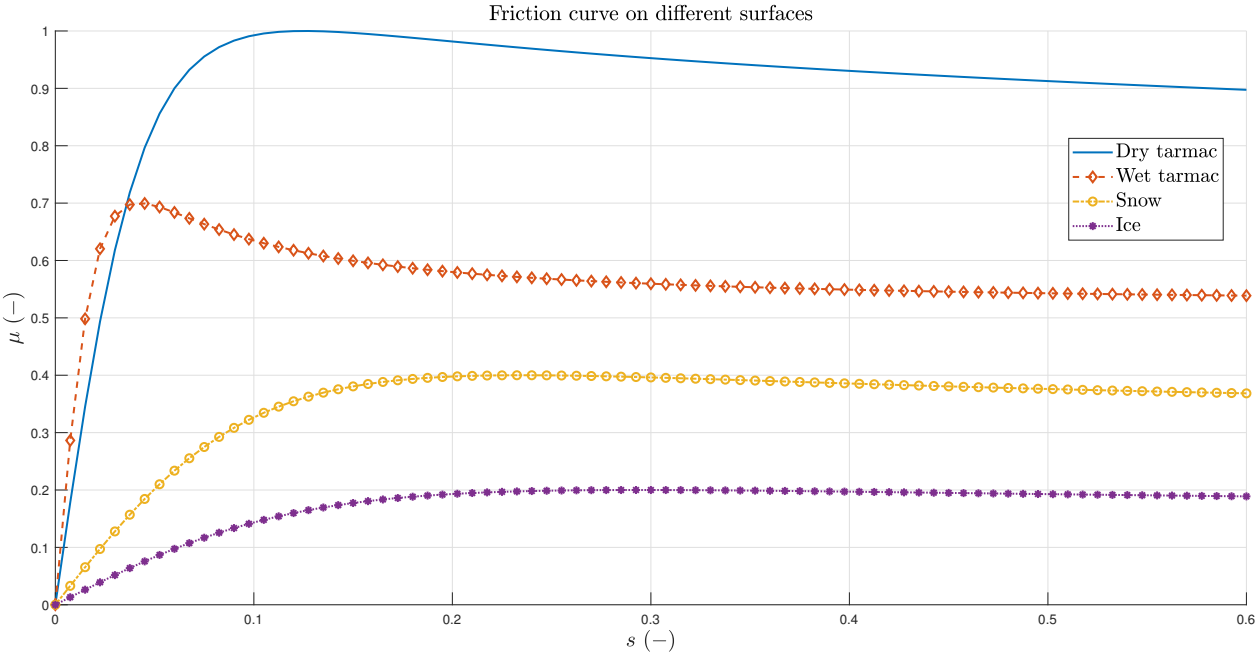

Figure 2: Example of curves representing the friction μ as a function of the slip ratio s.

In this contribution, a specific attention is paid to a parametric modelling approach because it can take into account the *a priori* knowledge about the tire behavior. More specifically, among the different tire models available in the literature [21, 25, 26, 17, 27], the very popular Pacejka's model [21] is selected because *(i)* it can represent the tire dynamics under various practical conditions accurately *(ii)* it is a parsimonious model, *i.e.* it has a limited number of parameters, which facilitates its use for parametric estimation. Such a model satisfies the following equation (see Figure 3 for a geometrical interpretation of the so-called "magic formula" parameters [21])

$$\mu = D \sin\left(C \arctan\left[Bx - E(Bx - \arctan(Bx))\right]\right) + s_v, \tag{5a}$$

$$x = s + s_h, \tag{5b}$$

or, in a compact way,

$$\mu = f(s, \boldsymbol{\theta}) \text{ with } \boldsymbol{\theta} = \begin{bmatrix} B & C & D & E & s_h & s_v \end{bmatrix}^\top, \tag{6}$$

where the corresponding "magic formula" parameters composing the unknown parameter vector $\boldsymbol{\theta} \in \mathbb{R}^{6\times 1}$ are defined in Table 2.

In a nutshell, by assuming that the user has access to

- (short and noisy) data sets $\{\mu_i, s_i\}_{i\in\{1,\cdots,N\}}$,
- a parametric model structure such as the Pacejka's model $f(\bullet, \boldsymbol{\theta})$,
- lower and upper bounds for each component of $\boldsymbol{\theta}$,

Table 2: Magic formula parameters.

Symbol	Definition
B	stiffness factor
C	shape factor
D	peak value
E	curvature factor
s_v	vertical shift
s_h	horizontal shift

our main goal is to estimate the parameter vector $\boldsymbol{\theta}$ accurately. As illustrated in Section 4, such a goal can be reached by resorting to the data driven model learning solutions introduced in the next section.

3. Pacejka's model learning: combining maximum likelihood and Monte Carlo Markov Chain

When parameter estimation of nonlinear static function from noisy data comes into play, the dominant solution in the literature consists in resorting to the maximum likelihood (ML) framework [28]. The ML solutions indeed benefit from interesting statistical properties like their asymptotic unbiasedness, efficiency and consistency under mild conditions [29, Chapter 3]. Such asymptotic properties can indeed help the user deliver reliable parameter estimates with quantification of the estimation accuracy [30]. As shown, *e.g.*, in [31], using asymptotic results to quantify model uncertainties from finite data sets can yield unreliable results when small size sets of data are used. This is the main reason why the Bayesian framework is nowadays often suggested to tackle parameter estimation problems when short data sets are handled [20]. The techniques involved in this framework, and more specifically the Monte Carlo (MC) random sampling methods [32], have the attractive property to give access to samples of a desired distribution (instead of a parameter vector as the ML solutions do) from user defined density function proposals by resorting to easy-to-implement algorithms mainly based on accept or reject conditions [33]. Interesting when short data sets are considered, as adviced in [34, Section 1], "it is important that we do not treat them as black boxes in order to obtain the best results out of this class of algorithms". This practical observation is probably the main reason why we suggest hereafter combining ML and MC algorithms to benefit from their respective advantages, *i.e.*, we tackle the problem of data driven model learning by using first a ML approach for get reliable initial guesses to tune, in a second step, a Monte Carlo Markov Chain (MCMC) algorithm. These two steps are more precisely introduced in the next sections.

3.1. Maximum likelihood: a short review

Because the tire friction is measured with (standard) sensors, the measured tire friction samples are assumed to be noisy. As a direct consequence, the model we consider from now on has the following form

$$\mu_i = f(s_i, \boldsymbol{\theta}) + e_i,\ i \in \{1, \cdots, N\}, \tag{7}$$

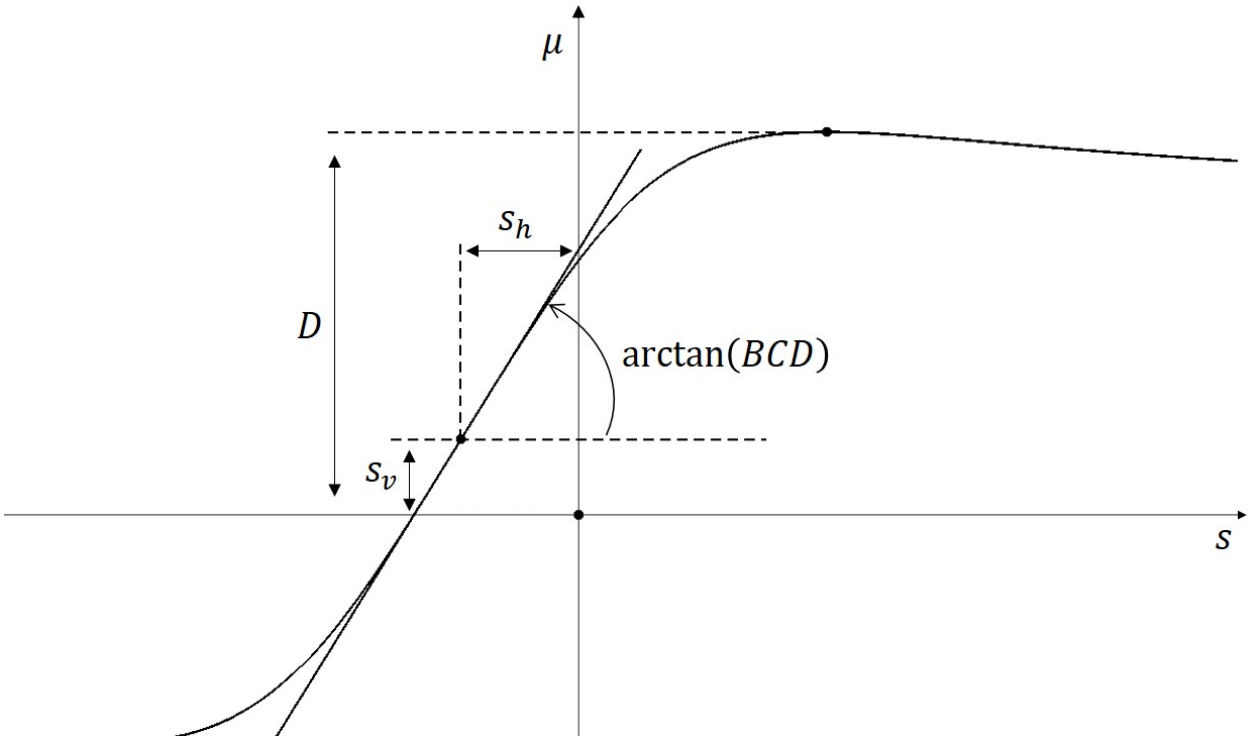

Figure 3: Example of tire friction curve calculated with Pacejka's formula and geometrical interpretation of the model parameters.

where e_i, $i \in \{1, \cdots, N\}$, stands for a sample of the realization $\boldsymbol{e}_1^N = (e_i)_{i\in\{1,\cdots,N\}}$ of a stochastic sequence $(\mathsf{e}_t)_{t\in\mathbb{Z}}$ characterized by a specific probability density function (pdf) $p_{\mathsf{e}}(\boldsymbol{e})$ [35]. Such an additive noise in the model description implies that the friction μ should also been considered as a random variable. Said differently, the acquired samples μ_i, $i \in \{1, \cdots, N\}$, are now seen as components of the realization $\boldsymbol{\mu}_1^N = (\mu_i)_{i\in\{1,\cdots,N\}}$ of the stochastic sequence $(\mu_t)_{t\in\mathbb{Z}}$. This observation is at the basis of the ML estimation solutions. More specifically, given the pdf of the random sequence $(\mu_t)_{t\in\mathbb{Z}}$ parameterized by $\boldsymbol{\theta}$, *i.e.*, given

$$p_{\boldsymbol{\mu}}(\boldsymbol{\mu}; \boldsymbol{s}, \boldsymbol{\theta}), \tag{8}$$

the maximum likelihood techniques aim at determining the unknown parameter vector $\boldsymbol{\theta}$ which "moves" this pdf such that it is maximum for our observed data or realization $(\mu_i)_{i\in\{1,\cdots,N\}}$. This probability density function $p_{\boldsymbol{\mu}}(\boldsymbol{\mu}; \boldsymbol{s}, \boldsymbol{\theta})$ evaluated at our observed data $\boldsymbol{\mu}_1^N = (\mu_i)_{i\in\{1,\cdots,N\}}$ acquired for the slip ratios $\boldsymbol{s}_1^N = (s_i)_{i\in\{1,\cdots,N\}}$, *i.e.*, $p_{\boldsymbol{\mu}}(\boldsymbol{\mu} = \boldsymbol{\mu}_1^N; \boldsymbol{s} = \boldsymbol{s}_1^N, \boldsymbol{\theta})$, is called the likelihood function and is denoted herein as follows

$$\ell(\boldsymbol{\mu}_1^N; \boldsymbol{s}_1^N, \boldsymbol{\theta}). \tag{9}$$

Thus, the maximum likelihood solutions estimate the parameter vector

$$\boldsymbol{\theta}_{\mathrm{ML}} = \arg\max_{\boldsymbol{\theta}} \ \ell(\boldsymbol{\mu}_1^N; \boldsymbol{s}_1^N, \boldsymbol{\theta}). \tag{10}$$

The solution of this maximization problem is strongly linked to the analytic equation of the likelihood function [30]. Because of the model structure given in Eq. (7), the likelihood function $\ell(\boldsymbol{\mu}_1^N; \boldsymbol{s}_1^N, \boldsymbol{\theta})$ is directly related to the noise probability density function $p_{\mathsf{e}}(\boldsymbol{e})$. More specifically, if it is assumed that the noise at each data point is independently distributed and zero mean, we have

$$\ell(\boldsymbol{\mu}_1^N; \boldsymbol{s}_1^N, \boldsymbol{\theta}) = \prod_{i \in \{1, \cdots, N\}} \mathcal{P}(f(s_i, \boldsymbol{\theta}), \sigma_i^2), \tag{11}$$

where σ_i^2, $i \in \{1, \cdots, N\}$, stands for the variance of component e_i, $i \in \{1, \cdots, N\}$, while $\mathcal{P}(\bullet_1, \bullet_2)$ is a generic notation for the noise probability density function of mean $\bullet_1$ and variance $\bullet_2$, respectively. Different popular continuous density functions can be suggested for $\mathcal{P}(\bullet_1, \bullet_2)$ [35]. In many practical cases, considering noise components which are

- conditionally independent,
- normally distributed with zero mean and with the same standard deviation σ,

is a reliable assumption. This is the main reason why we consider herein that

$$\ell(\boldsymbol{\mu}_1^N; \boldsymbol{s}_1^N, \boldsymbol{\theta}) = \prod_{i \in \{1, \cdots, N\}} \mathcal{N}(f(s_i, \boldsymbol{\theta}), \sigma^2), \tag{12}$$

where $\mathcal{N}(\bullet_1, \bullet_2)$ stands for the normal probability density function of mean $\bullet_1$ and variance $\bullet_2$, respectively. Because the natural logarithm is a monotonic increasing function, the maximum of $\ell(\boldsymbol{\mu}_1^N; \boldsymbol{s}_1^N, \boldsymbol{\theta})$ occurs at the same value of $\boldsymbol{\theta}$ as the maximum of the log-likelihood defined as follows

$$L(\boldsymbol{\mu}_1^N; \boldsymbol{s}_1^N, \boldsymbol{\theta}) = \log(\ell(\boldsymbol{\mu}_1^N; \boldsymbol{s}_1^N, \boldsymbol{\theta})) = -N \log(\sigma) - \frac{N}{2} \log(2\pi) - \frac{1}{2\sigma^2} V(\boldsymbol{\theta}), \tag{13}$$

with

$$V(\boldsymbol{\theta}) = \sum_{i=1}^{N} (\mu_i - f(s_i, \boldsymbol{\theta}))^2. \tag{14}$$

Such a direct relation between the (log-)likelihood and the least squares cost function $V(\boldsymbol{\theta})$ proves that maximizing $\ell(\boldsymbol{\mu}_1^N; \boldsymbol{s}_1^N, \boldsymbol{\theta})$ with respect to $\boldsymbol{\theta}$ boils down to minimizing $V(\boldsymbol{\theta})$ with respect to $\boldsymbol{\theta}$. The minimization of the cost function $V(\boldsymbol{\theta})$ requires the use of nonlinear optimization algorithms because of the nonlinear dependency of f with respect to $\boldsymbol{\theta}$. Several algorithms are available in the literature for minimizing $V(\boldsymbol{\theta})$ under such practical conditions [36, 37]. In this paper, the interior-reflective Newton method described in [38] (see also [36, Chapter 19]) is selected to reach a local optimum of $V(\boldsymbol{\theta})$ in order to take into the aforementioned lower and upper bounds on $\boldsymbol{\theta}$ explicitly during this numerical optimization.

Because the ML estimator is generated from noisy data, the estimated parameter vector $\boldsymbol{\theta}_{\mathrm{ML}}$ can be considered as a realization of a random vector $\boldsymbol{\Theta}_{\mathrm{ML}}$. As any random vector, $\boldsymbol{\Theta}_{\mathrm{ML}}$ can be characterized by standard (centered) moments [35] from which uncertainty domain or estimation quality certificates can be generated [39]. As proved, *e.g.*, in [30, Chapter 5], the asymptotic covariance matrix of the ML parameter estimator is

$$\mathrm{cov}(\boldsymbol{\Theta}_{\mathrm{ML}}) = \sigma^2 (\boldsymbol{F}_{\boldsymbol{\theta}_{\mathrm{ML}}}^{\top} \boldsymbol{F}_{\boldsymbol{\theta}_{\mathrm{ML}}})^{-1}, \tag{15}$$

where $\boldsymbol{F}_{\boldsymbol{\theta}_{\mathrm{ML}}}$ is the Jacobian matrix defined as

$$\boldsymbol{F}_{\boldsymbol{\theta}_{\mathrm{ML}}} = \begin{bmatrix} \frac{\partial f(s_1,\boldsymbol{\theta})}{\partial \theta_1} & \cdots & \frac{\partial f(s_1,\boldsymbol{\theta})}{\partial \theta_{n_\theta}} \\ \vdots & \ddots & \vdots \\ \frac{\partial f(s_N,\boldsymbol{\theta})}{\partial \theta_1} & \cdots & \frac{\partial f(s_N,\boldsymbol{\theta})}{\partial \theta_{n_\theta}} \end{bmatrix}_{\boldsymbol{\theta}=\boldsymbol{\theta}_{\mathrm{ML}}} \in \mathbb{R}^{N\times n_\theta}. \tag{16}$$

Furthermore, an unbiased estimate of σ^2 is given by [30, Chapter 5]

$$\hat{\sigma}^2 = \frac{V(\boldsymbol{\theta}_{\mathrm{ML}})}{N-n_\theta}. \tag{17}$$

These statistical results will be used in Section 4 for characterizing the estimation quality.

3.2. Adaptive Metropolis algorithms

While the minimization of $V(\boldsymbol{\theta})$ is feasible whatever the friction of data samples, the asymptotic statistical results of the ML estimator introduced previously may be not reliable when only low-friction data sets are handled (see Section *4.1.1* for an illustration of this claim). This is the main reason why the ML class of solutions should be combined with another class of methods when, as shown in Section 4, the friction data points remain under 0.3. The Bayesian framework, and more specifically the MC random sampling techniques, are used hereafter as a second step of our model learning solution because of their efficiency under such practical constraints [20]. By using again the fact that the unknown parameter vector $\boldsymbol{\theta}$ can be treated as a realization of a random vector $\boldsymbol{\Theta}$, the Bayesian inference solutions aim at determining the conditional or a posteriori probability density function $p_{\boldsymbol{\Theta},\boldsymbol{\mu}}(\boldsymbol{\theta} \mid \boldsymbol{\mu})$. More precisely, these solutions determine samples which form a distribution that asymptotically approaches $p_{\boldsymbol{\Theta},\boldsymbol{\mu}}(\boldsymbol{\theta} \mid \boldsymbol{\mu})$ [33]. Indeed, as shown hereafter, once these samples with common pdf are generated accurately, empirical means or covariance matrices can be computed effectively (see also [14]). In order to reach this goal, the heart of the Bayesian approach is the following pdf based Bayes formula [29]

$$p_{\boldsymbol{\Theta},\boldsymbol{\mu}}(\boldsymbol{\theta} \mid \boldsymbol{\mu}) = \frac{p_{\boldsymbol{\Theta},\boldsymbol{\mu}}(\boldsymbol{\mu} \mid \boldsymbol{\theta}) p_{\boldsymbol{\Theta}}(\boldsymbol{\theta})}{p_{\boldsymbol{\mu}}(\boldsymbol{\mu})}, \tag{18}$$

given two jointly distributed random vectors $\boldsymbol{\mu}$ and $\boldsymbol{\Theta}$, where [39]

- $p_{\boldsymbol{\Theta}}(\boldsymbol{\theta})$ stands for the prior pdf of $\boldsymbol{\Theta}$, *i.e.*, the belief we have on $\boldsymbol{\Theta}$ before seeing data,
- $p_{\boldsymbol{\Theta},\boldsymbol{\mu}}(\boldsymbol{\mu} \mid \boldsymbol{\theta})$ stands for the conditional pdf of $\boldsymbol{\mu}$ given $\boldsymbol{\theta}$, *i.e.*, our knowledge provided by $\boldsymbol{\mu}$ conditioned on knowing $\boldsymbol{\theta}$,
- $p_{\boldsymbol{\Theta},\boldsymbol{\mu}}(\boldsymbol{\theta} \mid \boldsymbol{\mu})$ stands for the posterior pdf we are interested in,
- $p_{\boldsymbol{\mu}}(\boldsymbol{\mu})$ stands for the marginal distribution of $\boldsymbol{\mu}$, *i.e.*,

$$p_{\boldsymbol{\mu}}(\boldsymbol{\mu}) = \int \cdots \int p_{\boldsymbol{\Theta},\boldsymbol{\mu}}(\boldsymbol{\mu} \mid \boldsymbol{\theta}) p_{\boldsymbol{\Theta}}(\boldsymbol{\theta}) d\boldsymbol{\theta}. \tag{19}$$

As far as our model learning problem is concerned, we assume the access to lower and upper bounds for each parameter. This prior is translated into a uniform flat prior $p_{\boldsymbol{\theta}}(\boldsymbol{\theta}) \propto 1$ within these bounds, *i.e.*,

$$\theta_i \sim \mathcal{U}([\theta_{i_{\text{lower}}}, \theta_{i_{\text{upper}}}]),\ i \in \{1, \cdots, n_\theta\}. \tag{20}$$

In addition, by assuming again zero mean independent and normally distributed measurement errors with a (known) constant variance σ^2, the conditional pdf $p_{\boldsymbol{\theta},\boldsymbol{\mu}}(\boldsymbol{\mu} \mid \boldsymbol{\theta})$ can be written as follows

$$p_{\boldsymbol{\theta},\boldsymbol{\mu}}(\boldsymbol{\mu} \mid \boldsymbol{\theta}) = \frac{1}{(2\pi\sigma^2)^{N/2}} \exp\left(-\frac{V(\boldsymbol{\theta})}{2\sigma^2}\right), \tag{21}$$

or, equivalently,

$$p_{\boldsymbol{\theta},\boldsymbol{\mu}}(\boldsymbol{\mu} \mid \boldsymbol{\theta}) \propto \exp\left(-\frac{V(\boldsymbol{\theta})}{2\sigma^2}\right). \tag{22}$$

Remark 1. *As pointed out,* e.g.*, in [39], this pdf is identical in form to the likelihood function introduced previously. In the Bayesian case, the pdf is however a conditional pdf while, in the ML approach, the pdf is an unconditional pdf parameterized by* $\boldsymbol{\theta}$.

In a nutshell, for our model learning problem,

$$p_{\boldsymbol{\theta},\boldsymbol{\mu}}(\boldsymbol{\theta} \mid \boldsymbol{\mu}) \propto \frac{\exp\left(-\frac{V(\boldsymbol{\theta})}{2\sigma^2}\right)}{p_{\boldsymbol{\mu}}}. \tag{23}$$

The challenging step in the Bayesian approach is the determination of $p_{\boldsymbol{\mu}}$. Indeed, in most of practical cases, the multiple integrals involved in the definition of $p_{\boldsymbol{\mu}}$ cannot be computed analytically while standard numerical integration methods [40] fail when n_θ is larger than a few [34]. Fortunately, the class of Metropolis-Hastings (MH) algorithms [41] allows to sample a pdf on condition that this distribution is known up to a multiplicative constant. Indeed, with the MH algorithm, new samples $\boldsymbol{\theta}^{(i)}$ are generated from a user defined proposal distribution, then accepted or rejected according to a simple rule involving the acceptance probability ratio defined as follows

$$\alpha^{(i)} = \frac{p_{\boldsymbol{\theta},\boldsymbol{\mu}}(\boldsymbol{\theta}^{(i)} \mid \boldsymbol{\mu})}{p_{\boldsymbol{\theta},\boldsymbol{\mu}}(\boldsymbol{\theta}^{(i-1)} \mid \boldsymbol{\mu})} = \frac{p_{\boldsymbol{\theta},\boldsymbol{\mu}}(\boldsymbol{\mu} \mid \boldsymbol{\theta}^{(i)}) p_{\boldsymbol{\theta}}(\boldsymbol{\theta}^{(i)})}{p_{\boldsymbol{\theta},\boldsymbol{\mu}}(\boldsymbol{\mu} \mid \boldsymbol{\theta}^{(i-1)}) p_{\boldsymbol{\theta}}(\boldsymbol{\theta}^{(i-1)})}. \tag{24}$$

Because $\alpha^{(i)}$ is a ratio of posterior distribution, it does not involve $p_{\boldsymbol{\mu}}$. As a direct consequence for our model learning problem, a MH algorithm can be used hereafter to generate samples from this posterior distribution. Among the MH algorithms available in the literature (see, *e.g.*, [20] for a recent list of MH solutions), the starting point of our solution is the random walk Metropolis algorithm [20, Section 3.1.1]. This specific choice is dictated by the facts that

- for the random walk Metropolis algorithm, the aforementioned proposal distribution can be a Gaussian pdf centered on the current candidate, *i.e.*, the candidate parameter vector can be easily generated with standard random number generators once an initial parameter covariance matrix is selected by the user,

- this algorithm satisfies the convergence constraints to guarantee that, asymptotically, the selected samples approach the correct expected values, *i.e.*, share the same pdf and, more importantly, this pdf is $p_{\boldsymbol{\theta},\boldsymbol{\mu}}(\boldsymbol{\theta} \mid \boldsymbol{\mu})$ (see [34, Section 3.1] or [41, Chapter 7] for a proof of this claim).

While the core of the random walk Metropolis algorithm is made of 5 lines or so (see, *e.g.* [32, Chapter 6], as well as Algorithm 1), the efficiency of our MH algorithm is strongly linked to practical tips and hints[3] for monitoring or adapting it (like any other MH algorithms in fact (see, *e.g.*, [32, Chapter 8] for an interesting list of MH algorithm improvements)). More specifically, herein, the standard random walk MH algorithm is refined by

- running n_{mc} Markov chains with different initializations in parallel in order to assess if they all converge towards the same distribution. The initialization guesses of each Markov are either generated by using the ML estimates (parameter vector and covariance matrix) or by randomly generating parameter vectors within the user defined parameter lower and upper bounds with a uniform distribution for instance. The procedure used to test the convergence of the Markov chains is based on the "within and between sequence variances" approach borrowed from [42, Section 11.4];
- keeping the different Markov chains, then "burning in" [14, Section 9.4], *i.e.*, throwing away the samples used during this initialization of the Markov chains;
- resuming the random walk MH algorithm for the different Markov chains,
- adapting the covariance matrix used by the random walk MH algorithm by
  - computing first an empiric covariance matrix once enough samples have been generated,
  - updating the covariance matrix after each sample generated following the expression introduced by Vihola [43] and recalled by Särkkä in [44, Section 12.2.2],
- "thinning" [14, Section 9.4], *i.e.*, removing samples in order to keep a chain of uncorrelated samples.

Such steps are summed in Algorithm 1.

Remark 2. *As indicated in Algorithm 1, the random walk MH algorithm is performed on n_{mc} Markov chains. By doing so, the method provides n_{mc} estimates that can be gathered into histograms. However, after assessing that the different chains converge to the same distribution, it is common to select one chain and thus to have one mean estimation. One way to select the chain is to keep the chain which has the acceptance rate the closest to the ideal acceptance rate for the random walk MH defined by $\bar{\alpha}_* = 0.234$ [44]. In the case treated here, the estimation procedure is applied with low friction measurements. For this reason, the*

[3] As shown in [34], "in order to obtain best results out of this class of algorithms", the user must "incorporate as much domain specific knowledge as possible into their design".

Algorithm 1 MCMC based estimation method

Inputs:

- $\boldsymbol{\theta}_{lower}, \boldsymbol{\theta}_{upper}$: parameter bounds
- M: chain lengths
- n_{mc}: number of chains
- n_{ML}: number of initial guesses for ML estimation

Outputs:

- n_{mc} estimates $\boldsymbol{\theta}_{\text{MCMC}}$
- n_{mc} estimates of μ_{max}

Generate n_{ML} initial guesses $\boldsymbol{\theta}^{(0)}$ by picking values randomly according to a uniform distribution between the parameter bounds
Estimate n_{ML} parameter vectors $\boldsymbol{\theta}_{\text{ML}}$ with the ML method
Keep the parameter vector $\boldsymbol{\theta}_{\text{ML}}$ giving the smallest residual norm $V(\boldsymbol{\theta})$ defined in Eq. (14) and estimate the covariance matrix $\boldsymbol{\Sigma}_{\text{ML}}$ defined in Eq. (15)

} Maximum Likelihood

Initialize n_{mc} chains at the value $\boldsymbol{\theta}_{\text{ML}}$ and the initial covariance matrix $\boldsymbol{\Sigma}^{(0)}$ at the value $\boldsymbol{\Sigma}_{\text{ML}}$
Initialize $\boldsymbol{S}^{(0)}$ to be the lower-triangular Cholesky factor of the initial covariance $\boldsymbol{\Sigma}^{(0)}$
for $i = 1$ to M **do**
    Sample a new candidate, *i.e.*, $\boldsymbol{\theta}^* = \boldsymbol{\theta}^{(i-1)} + \boldsymbol{S}^{(i-1)}\boldsymbol{r}^{(i)}$, where $\boldsymbol{r}^{(i)} \sim \mathcal{N}(0, I)$
    Compute the acceptance probability $\alpha^{(i)}$
    Sample a uniform random variable $u \sim \mathcal{U}(0, 1)$
    If $u \leq \alpha^{(i)}$, accept the sample and set $\boldsymbol{\theta}^{(i)} = \boldsymbol{\theta}^*$, otherwise, reject the sample and set $\boldsymbol{\theta}^{(i)} = \boldsymbol{\theta}^{(i-1)}$

} Core of MH algorithm

    Compute a lower-triangular matrix $\boldsymbol{S}^{(i)}$ with positive diagonal elements satisfying the equation

$$\boldsymbol{S}^{(i)}\boldsymbol{S}^{(i)^\top} = \boldsymbol{S}^{(i-1)}\left(I + \eta^{(i)}(\alpha^{(i)} - \bar{\alpha_*})\frac{\boldsymbol{r}^{(i)}\boldsymbol{r}^{(i)^\top}}{||\boldsymbol{r}^{(i)}||^2}\right)\boldsymbol{S}^{(i-1)^\top},$$

    where $\eta^{(i)} \in [0, 1]$ is an adaptation step size sequence decaying to zero (*e.g.* $\eta^{(i)} = i^{-\gamma}$ with $\gamma \in [0.5, 1]$) and $\bar{\alpha_*} = 0.234$ the ideal acceptance probability

} Covariance adaptation from [44]

Thin the different chains to keep chains of uncorrelated samples
Compute an estimate $\boldsymbol{\theta}_{\text{MCMC}}$ for each chain using Equation (25)
Estimate n_{mc} friction curves with the n_{mc} estimates $\boldsymbol{\theta}_{\text{MCMC}}$ by using Eq. (26)
Determine the maximum of each friction curves

estimates obtained are more likely to vary from one simulation to another. Thus it can be difficult to select one chain among all. Therefore, all the n_{mc} Markov chains are kept in this study.

Once reliable chain samples are generated, the parameters estimation can be done using the expression [14]

$$\boldsymbol{\theta}_{\text{MCMC}} = \mathbb{E}_{p_{\boldsymbol{\theta},\boldsymbol{\mu}}(\boldsymbol{\theta}|\boldsymbol{\mu})}(\boldsymbol{\theta} \mid \boldsymbol{\mu}) = \int \cdots \int \boldsymbol{\theta} p_{\boldsymbol{\theta},\boldsymbol{\mu}}(\boldsymbol{\theta} \mid \boldsymbol{\mu}) d\boldsymbol{\theta} \approx \frac{1}{Mn_{\text{mc}}} \sum_{j=1}^{Mn_{\text{mc}}} \boldsymbol{\theta}^{(j)}. \tag{25}$$

In others words, the parameters estimation is made by averaging the available samples. Finally, the prediction on an unseen point $\{s_{M+1}, \mu_{M+1}\}$ can be carried out as follows [14]

$$\mu_{M+1} = \mathbb{E}_{p_{\boldsymbol{\theta},\boldsymbol{\mu}}(\boldsymbol{\theta}|\boldsymbol{\mu})}(f(\boldsymbol{\theta}, s_{M+1}) \mid \boldsymbol{\mu}) \approx \frac{1}{Mn_{\text{mc}}} \sum_{j=1}^{Mn_{\text{mc}}} f(\boldsymbol{\theta}^{(j)}, s_{M+1}). \tag{26}$$

Because the slip ratio corresponding to the tire-road friction μ_{max} is not known *a priori*, Equation (26) cannot be used directly to estimate μ_{max}. However, this equation can be used with many slip ratio to draw the entire friction curve. Once the curve is obtained, μ_{max} is determined straightforwardly by taking the maximum of the friction curve or by examining when the derivative of the friction curve with respect to the slip ratio is equal to zero.

4. Case studies

In this section, the MCMC model learning technique performance is assessed with both simulated data (Section *4.1*) and real data (Section *4.2*). Because in Section *4.1*, the measurements are simulated, we have access to the real parameter vector $\boldsymbol{\theta}$. Thus the estimated values obtained with the MCMC[4] method can be compared to the actual values directly. For this reason, Section *4.1* focuses on the ability of the method to estimate the parameter vector $\boldsymbol{\theta}$ rather than the friction potential. If $\boldsymbol{\theta}$ is estimated accurately, the estimated grip potential determined, *e.g.*, by computing the derivative $\frac{\partial f}{\partial s}$, should indeed be reliable as well. In Section *4.2*, we use on the contrary real measurements of the friction potential generated with a flat track tire testing machine [45]. Under such practical conditions, we do not have access to the real parameter vector $\boldsymbol{\theta}$. Hence, the method performance is assessed by comparing the estimated grip potential with a grip potential extracted from the real measurements only.

4.1. Results with simulated data

In order to evaluate the effectiveness of the estimation method introduced in this paper, the MCMC model learning method is first tested with simulated data. The results obtained with the MCMC model learning method are compared with the ones obtained with the ML method carried out on the same simulated data.

[4]In the following, the MCMC method refers to the method described in Algorithm 1, *i.e.*, the adaptive MCMC initialized with ML estimate.

The simulated data is generated with the Pacejka's tire model given in Eq. (5) disturbed with an output zero mean white Gaussian noise characterized by a standard deviation σ equal to 2.53e-2 (see Figure 4). This standard deviation value corresponds to a signal-to-noise ratio equal to 15 dB. The value of the standard deviation is set regarding the real friction data used in Section *4.2*. Here, the simulated measurements correspond to a situation frequently encountered in practice, namely a tire rolling on a dry road. The ML and MCMC methods are tested with 3 different training sets. The first two training sets contain only simulated measurements for $\mu \leq 0.3$ and $\mu \leq 0.6$, respectively. The third training set contains all the data points for $s \in [0, 0.4]$.

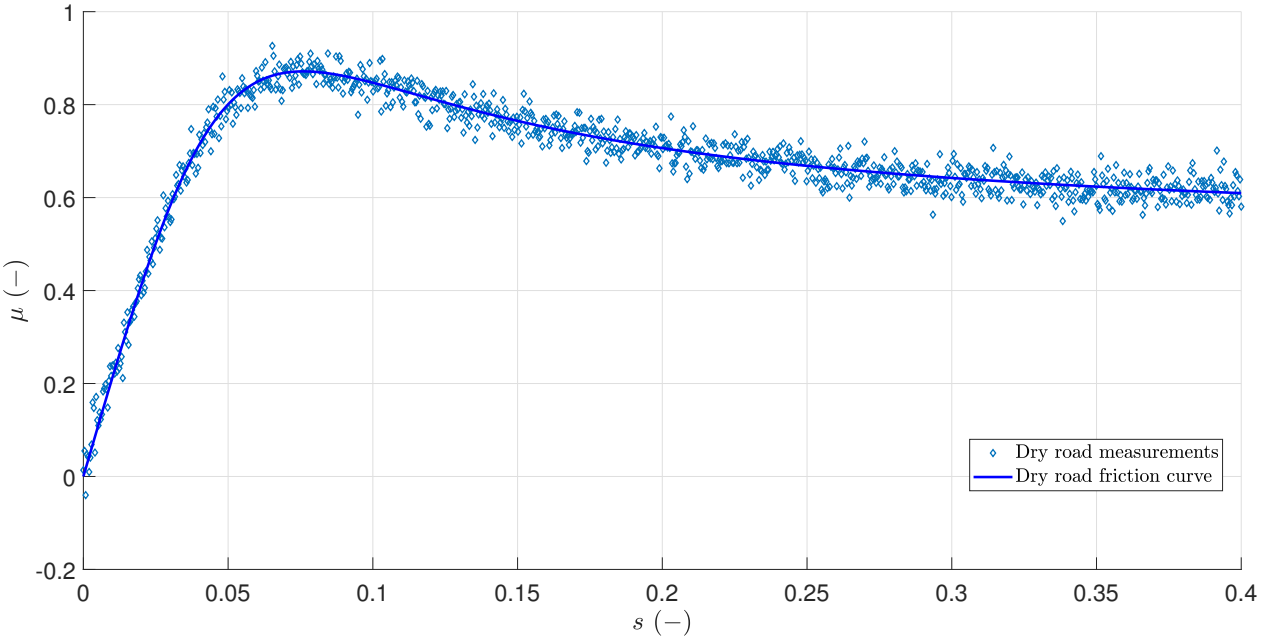

Figure 4: Friction simulated measurements generated with the Pacejka's tire model.

4.1.1. Results with the Maximum Likelihood method

The ML method is first tested with the aforementioned simulated training sets. In the different cases treated here, the ML method is performed 10000 times ($n_{ML} = 10000$ in Algorithm 1) with 10000 different initial guesses. As indicated in Algorithm 1, the different initial guesses $\boldsymbol{\theta}^{(0)}$ are generated randomly according to a uniform distribution between the parameter bounds. Here, the bounds, given in Table 3, are taken so that the Pacejka's model can generate realistic friction curves corresponding to any kind of situations such as a vehicle driving on dry asphalt, wet asphalt or even icy road [46].

Under these conditions, the ML method provides 10000 estimates of the parameter vector $\boldsymbol{\theta}$. These estimates are represented in Figures 5, 6 and 7, respectively. In addition, these Figures also include a Gaussian pdf fitted to the 10000 estimates. More precisely, the means and the standard deviations of the pdf are determined by computing the means and the standard deviations of the 10000 estimates obtained with each training set.

Table 3: Intervals of Pacejka's parameters.

Parameter	Lower and upper bound
B	$[5, 30]$
C	$[0.5, 2]$
D	$[0.2, 2]$
E	$[-2, 0]$
s_h	$[-0.05, 0.05]$
s_v	$[-0.3, 0.3]$

Among the 10000 estimates, different estimated values are also extracted. Firstly, the mean of the 10000 estimates. Secondly, the estimated parameter vector $\boldsymbol{\theta}_{\mathrm{ML}}$ giving the smallest residual norm $V(\boldsymbol{\theta})$ defined in Eq. (14). In the following, this second estimate is referred as "Minimizer of the loss function". These two estimated values are represented in Figure 5, 6 and 7 and are summarized in Table 4. Furthermore, the ML method provides estimates of the measurement standard deviation (see Eq. (17)). These estimates are gathered and compared with the actual value in Table 5. Finally, covariance matrices of the parameter vector are given in Table 6. In this Table, two types of covariance matrices are reported, (i) the theoretical covariance matrices computed with Equation (15), (ii) empirical covariance matrices obtained by computing the covariance of the 10000 estimates.

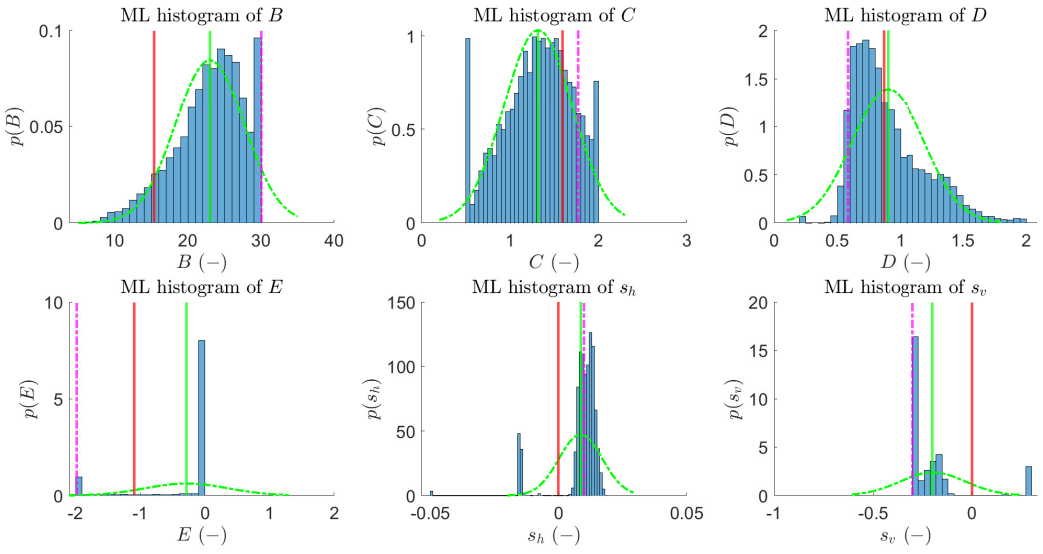

Figure 5: Histograms of the Pacejka's parameters estimated with the ML method (for $\mu \leq 0.3$). The red line represents the true value used to generate the friction measurements. The green line indicates the mean of the ML estimates. The magenta dash-dot line indicates the minimizer of the loss function. The green dash-dot line represents a Gaussian pdf fitted to the 10000 ML estimates.

Table 4: ML estimates with simulated data. The relative error lines give the relative errors between the different estimates and the true parameter values.

	B	C	D	E	s_h	s_v
True value	15.4	1.60	$8.71e-1$	-1.09	0	0
Friction limit : $\mu = 0.30$						
Mean of the estimates	23.0	1.32	$9.04e-1$	$-2.84e-1$	$8.61e-3$	$-1.99e-1$
(Relative error)	49.3%	17.43%	3.76%	74.0%	–	–
Minimizer of the loss function	30.0	1.77	$5.83e-1$	-1.98	$9.98e-3$	$-3.00e-1$
(Relative error)	94.8%	11.1%	33.1%	81.9%	–	–
Friction limit : $\mu = 0.60$						
Mean of the estimates	28.4	1.21	$6.22e-1$	-1.84	$-6.53e-3$	$1.48e-1$
(Relative error)	84.5%	24.1%	28.6%	68.7%	–	–
Minimizer of the loss function	30.0	1.21	$5.39e-1$	-2.00	$-7.71e-3$	$1.72e-1$
(Relative error)	94.8%	24.3%	38.1%	83.3%	–	–
Without friction limit						
Mean of the estimates	15.9	1.63	$8.00e-1$	$-9.57e-1$	$-2.76e-3$	$6.96e-2$
(Relative error)	3.44%	2.20%	8.25%	12.2%	–	–
Minimizer of the loss function	17.0	1.67	$7.09e-1$	$-6.44e-1$	$-7.11e-3$	$1.60e-1$
(Relative error)	10.4%	4.61%	18.6%	41.0%	–	–

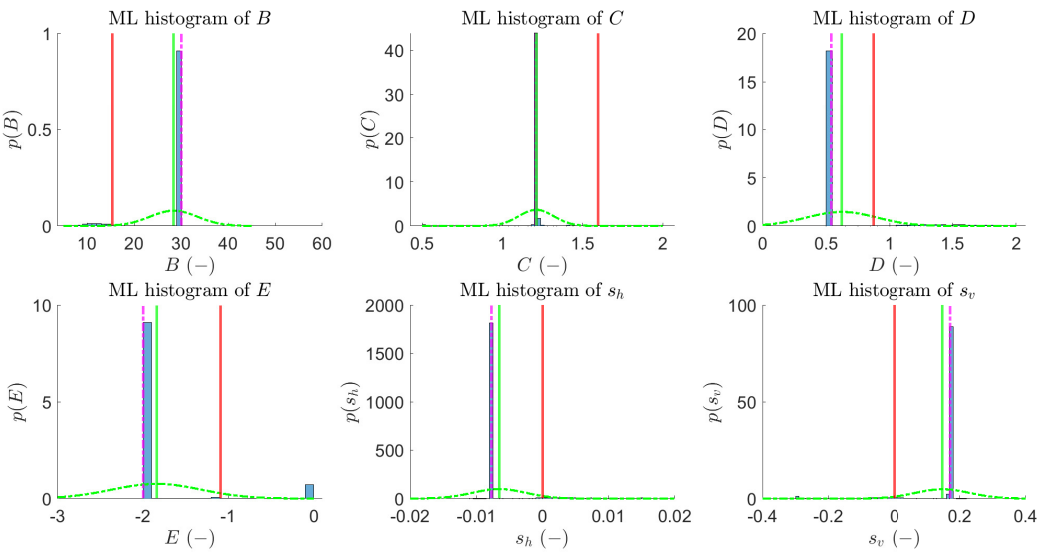

Figure 6: Histograms of the Pacejka's parameters estimated with the ML method (for $\mu \leq 0.6$). The red line represents the true value used to generate the friction measurements. The green line indicates the mean of the ML estimates. The magenta dash-dot line indicates the minimizer of the loss function. The green dash-dot line represents a Gaussian pdf fitted to the 10000 ML estimates.

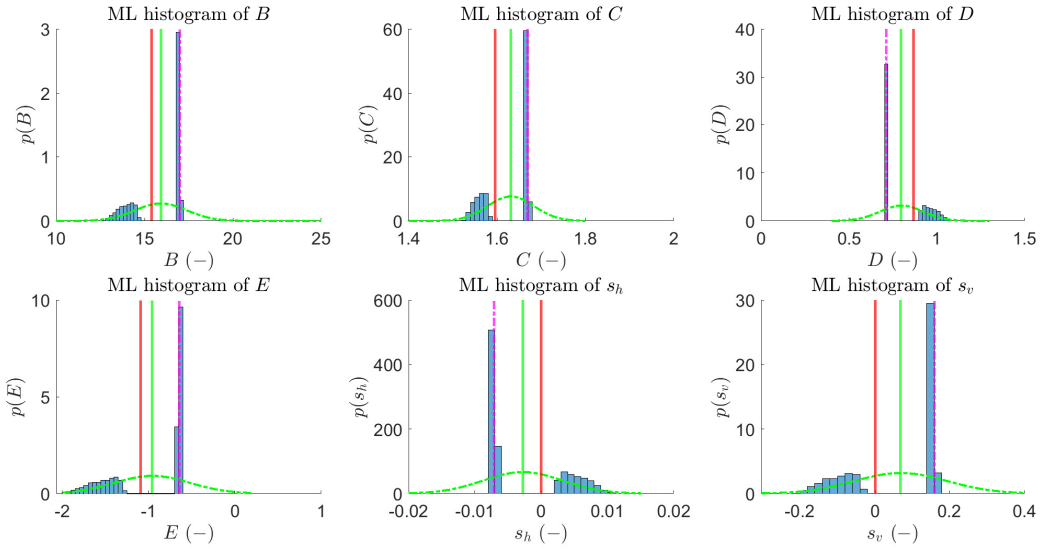

Figure 7: Histograms of the Pacejka's parameters estimated with the ML method (all data points selected). The red line represents the true value used to generate the friction measurements. The green line indicates the mean of the ML estimates. The magenta dash-dot line indicates the minimizer of the loss function. The green dash-dot line represents a Gaussian pdf fitted to the 10000 ML estimates.

As illustrated in Figure 5, 6 and 7, the means of the 10000 estimates are different from the minimizers

Table 5: Measurement standard deviation estimated with the ML method. The relative error lines give the relative errors between the different estimates and the true value.

	σ
True value	$2.53e-2$
Friction limit : $\mu = 0.30$	
ML	$3.32e-2$
(Relative error)	30.9%
Friction limit : $\mu = 0.60$	
ML	$2.96e-2$
(Relative error)	16.8%
Without friction limit	
ML	$2.53e-2$
(Relative error)	0%

of the loss function. In addition, the mean estimates are closer to the actual parameter values than the minimizers of the loss function. However, in the first two cases (measurements limited by $\mu < 0.3$ and $\mu < 0.6$, respectively), the mean estimates and the minimizer of the loss function are far from the actual values. On the contrary, when all the data points are considered, the ML method provides accurate estimates of the parameters. Besides, in this case, the measurement standard deviation supplied by the ML method is equal to the actual value used to simulate the data (see Table 5). Furthermore, in the first two cases, the Jacobian matrices $\boldsymbol{F}_{\boldsymbol{\theta}_{\mathrm{ML}}}$ given in Eq. (16) are ill-conditioned. For this reason, the theoretical covariance matrices (see Eq. (15)) computed by using the Jacobian matrices $\boldsymbol{F}_{\boldsymbol{\theta}_{\mathrm{ML}}}$, contain huge values as reported in Table 6. On the opposite, when the last training set is considered, the Jacobian matrix $\boldsymbol{F}_{\boldsymbol{\theta}_{\mathrm{ML}}}$ is not ill-conditioned. Thus, in this case, the theoretical covariance matrix has realistic values and is almost equal to the covariance matrix computed with the 10000 ML estimates.

All these results indicate that the ML method is suitable when data points describing the entire friction curve are available. However, when only training sets containing low friction measurements are at disposal, the ML method provides poor results. For this reason, another estimation method is needed under standard driving conditions.

4.1.2. Results with the MCMC method

The MCMC based estimation method is now tested with the different training sets described in the paragraph before the Section *4.1.1.* As indicated in Algorithm 1, the MCMC model learning method requires

Table 6: Parameters covariance matrices obtained with the ML method. The theoretical column corresponds to the covariance matrices computed with Eq. (15). The empirical covariance matrices corresponds to the covariance matrices computed with the 10000 estimates.

Theoretical	Empirical
Friction limit : $\mu = 0.30$	
$\begin{bmatrix} 59679083 & 617642 & -1334586 & 10420621 & -43759 & 1337187 \\ 617642 & 6652 & -13866 & 108781 & -455 & 13890 \\ -1334586 & -13866 & 29857 & -233222 & 979 & -29914 \\ 10420621 & 108781 & -233222 & 1822970 & -7648 & 233667 \\ -43759 & -455 & 979 & -7648 & 32 & -981 \\ 1337187 & 13890 & -29914 & 233667 & -981 & 29972 \end{bmatrix}$	$\begin{bmatrix} 22.2905 & 0.0366 & -0.6287 & -0.0111 & -0.0048 & -0.0122 \\ 0.0366 & 0.1500 & -0.0891 & 0.0894 & 0.0011 & -0.0297 \\ -0.6287 & -0.0891 & 0.0823 & -0.0642 & -0.0005 & 0.0166 \\ -0.0111 & 0.0894 & -0.0642 & 0.4112 & 0.0041 & -0.0799 \\ -0.0048 & 0.0011 & -0.0005 & 0.0041 & 0.0001 & -0.0013 \\ -0.0122 & -0.0297 & 0.0166 & -0.0799 & -0.0013 & 0.0278 \end{bmatrix}$
Friction limit : $\mu = 0.60$	
$\begin{bmatrix} 215526.65 & -10463.68 & 800.89 & 16267.38 & -48.61 & 952.37 \\ -10463.68 & 527.43 & -47.37 & -789.87 & 2.16 & -42.26 \\ 800.89 & -47.37 & 6.69 & 60.58 & -0.09 & 1.80 \\ 16267.38 & -789.87 & 60.58 & 1235.65 & -3.68 & 72.16 \\ -48.61 & 2.16 & -0.09 & -3.68 & 0.01 & -0.26 \\ 952.37 & -42.26 & 1.80 & 72.16 & -0.26 & 5.04 \end{bmatrix}$	$\begin{bmatrix} 25.4821 & -0.1198 & -1.2810 & -2.5468 & -0.0190 & 0.3863 \\ -0.1198 & 0.0119 & -0.0040 & 0.0066 & 0.0000 & -0.0008 \\ -1.2810 & -0.0040 & 0.0754 & 0.1309 & 0.0010 & -0.0212 \\ -2.5468 & 0.0066 & 0.1309 & 0.2759 & 0.0018 & -0.0359 \\ -0.0190 & 0.0000 & 0.0010 & 0.0018 & 0.0000 & -0.0003 \\ 0.3863 & -0.0008 & -0.0212 & -0.0359 & -0.0003 & 0.0069 \end{bmatrix}$
Without friction limit	
$\begin{bmatrix} 2.3744 & 0.0952 & -0.1696 & 0.5560 & -0.0084 & 0.1685 \\ 0.0952 & 0.0039 & -0.0070 & 0.0224 & -0.0003 & 0.0069 \\ -0.1696 & -0.0070 & 0.0124 & -0.0396 & 0.0006 & -0.0124 \\ 0.5560 & 0.0224 & -0.0396 & 0.1335 & -0.0020 & 0.0393 \\ -0.0084 & -0.0003 & 0.0006 & -0.0020 & 0.0000 & -0.0006 \\ 0.1685 & 0.0069 & -0.0124 & 0.0393 & -0.0006 & 0.0123 \end{bmatrix}$	$\begin{bmatrix} 2.1736 & 0.0774 & -0.1844 & 0.6428 & -0.0088 & 0.1841 \\ 0.0774 & 0.0028 & -0.0066 & 0.0229 & -0.0003 & 0.0066 \\ -0.1844 & -0.0066 & 0.0157 & -0.0546 & 0.0008 & -0.0156 \\ 0.6428 & 0.0229 & -0.0546 & 0.1905 & -0.0026 & 0.0545 \\ -0.0088 & -0.0003 & 0.0008 & -0.0026 & 0.0000 & -0.0007 \\ 0.1841 & 0.0066 & -0.0156 & 0.0545 & -0.0007 & 0.0156 \end{bmatrix}$

the initialization of some quantities. Namely, the chain lengths, the chain numbers and the parameter bounds. Herein, the MCMC method developed in Section 3 is performed with 100 chains to obtain 100 estimates of $\boldsymbol{\theta}$. Each chain has a length of 50 000 samples. Besides the parameter bounds are the ones given in Table 3.

Remark 3. *At this point, the previous settings should be sufficient for performing the MCMC based estimation method (see Algorithm 1). However, in our case, the Jacobian matrices $\boldsymbol{F}_{\boldsymbol{\theta}_{ML}}$ obtained with the ML method carried out on the two first training sets are ill-conditioned (see Section 4.1.1). As a consequence, the theoretical ML covariance matrices estimated are not suitable for initializing the covariance matrix of the MCMC proposal distribution in these two cases. The proposal covariance matrix should indeed be set so that the generated samples browse the parameters space properly [14]. The most important factor influencing the sample generation is the variance of the parameters. In the proposal covariance matrix, the parameter variances are representing by the diagonal elements. For this reason, the proposal covariance matrix is chosen diagonal. Besides, the magnitude of the diagonal elements is set regarding the ML covariance matrix estimated when all the data points are selected. Finally, the diagonal elements are set to higher values than the ML matrix. The diagonal values are higher so that the generated samples cover a wider space. As a consequence, the initial covariance matrix of the proposal distribution is set as follows*

$$\boldsymbol{\Sigma}^{(0)} = diag\,(7, 0.43, 0.3, 0.3, 0.005, 0.01)\,. \tag{27}$$

Under such practical conditions, the MCMC based estimation method provides the results given in Figures 8, 9 and 10 and sum up in Table 7. The MCMC estimated values gathered in Table 7 correspond to the mean of the 100 estimates. In addition, Gaussian pdf have been fitted to the MCMC estimates. The means and the standard deviations used to fit the pdf correspond to the means and the standard deviations of the 100 estimates.

Table 7: MCMC estimates with simulated data. The relative error lines give to the relative errors between the different estimates and the true parameter values.

	B	C	D	E	s_h	s_v
True value	15.4	1.60	$8.71e-1$	-1.09	0	0
Friction limit : $\mu = 0.30$						
MCMC	17.5	1.24	1.03	-1.03	$2.41e-3$	$-1.67e-2$
(Relative error)	13.7%	22.1%	18.2%	5.97%	–	–
Friction limit : $\mu = 0.60$						
MCMC	16.3	1.21	1.21	$-9.80e-1$	$4.20e-4$	$6.25e-3$
(Relative error)	6.03%	24.0%	38.7%	10.2%	–	–
Friction limit : all points						
MCMC	16.6	1.62	$8.09e-1$	$-9.31e-1$	$-2.14e-3$	$5.29e-2$
(Relative error)	7.70%	1.39%	7.19%	14.68%	–	–

As illustrated in Figures 8, 9 and 10 (see also Table 7), the MCMC model learning method outperforms the ML method for all scenarii. For the three different cases, the MCMC estimates are indeed closer to the true values than the ones obtained with the ML method. Besides, we can note that the MCMC estimates obtained with a friction limit of 0.3 are closer to the actual values (except for B) than the ones obtained with a friction limit of 0.6.

To conclude this part, the MCMC model learning technique provides interesting results to estimate the parameters of the Pacejka's tire model and outperforms the ML method. Thus, it is now time to test the ML and the MCMC methods on real data with realistic friction measurement sets.

4.2. Results with real data

In this section, the method described in Section 3 is tested with real data coming from a flat track tire testing machine. A flat track tire testing machine is a machine allowing the user to conduct experiments

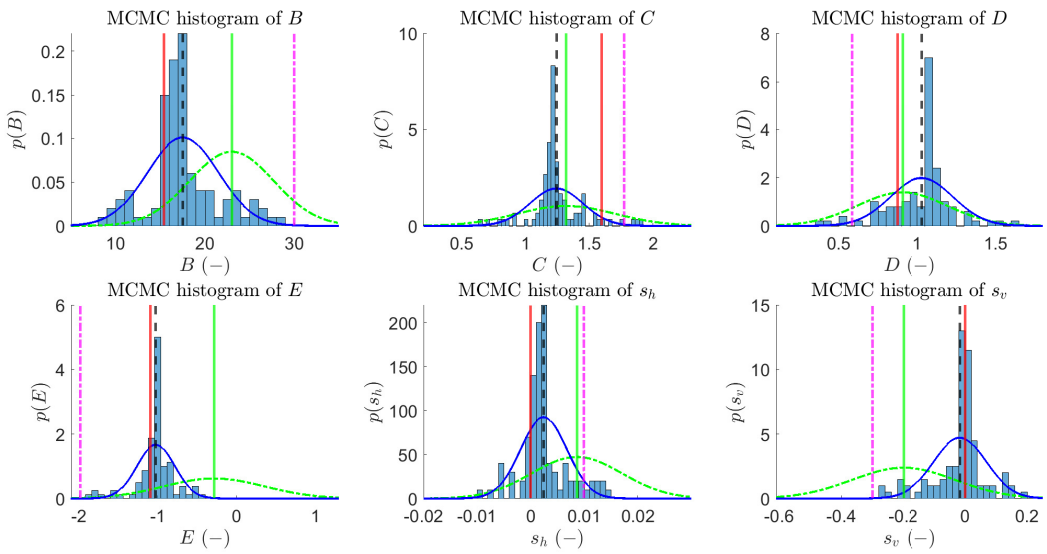

Figure 8: Histograms of the Pacejka's parameters estimated with the MCMC method (for $\mu \leq 0.3$). The red line represents the true value used to generate the friction measurements. The black dashed line indicates the mean of the MCMC estimates. The magenta dash-dot line indicates the minimizer of the loss function. The green line indicates the mean of the ML estimates. The blue line represents a Gaussian pdf fitted to the MCMC estimates. The green line represents a Gaussian pdf fitted to the 10000 ML estimates.

on a tire by applying specific constraints like a desired normal load or by rolling the tire at a desired speed [45]. Therefore, a flat track tire testing machine offers the possibility to collect useful information on the tire behavior by studying its dynamical responses. Among the signals available thanks to the flat track tire testing machine, we can have access to the slip ratio s as well as the tire forces F_x, F_y and F_z respectively. Hence, by using Eq. (1), we obtained the friction measurements given in Figure 11.

In Figure 11, it can be pointed out that the friction measurements depict the entire friction curve which is not available under standard practical driving conditions. Here, all these data points are accessible because the flat track offers the possibility to impose high slip ratios to the tire and thus allows the acquisition of the tire response for a large range of slip ratio. As a consequence, these representative measurements offer the opportunity to test the MCMC based estimation method and the ML method on different part of the friction curve.

4.2.1. Tests with full measurements

In the first scenario, the method is applied using the full data sets for $s \in [0, 0.2]$. Although this situation does not correspond to classical driving conditions, this test enables to check if the method can provide good results under ideal situations. In the same way as we proceeded in the case with simulated data, the MCMC based estimation method is applied with a high number of chains to ensure a satisfying efficiency of the method. Here the number of chains is set to 300 which imply 300 estimates of the grip potential. Each chain

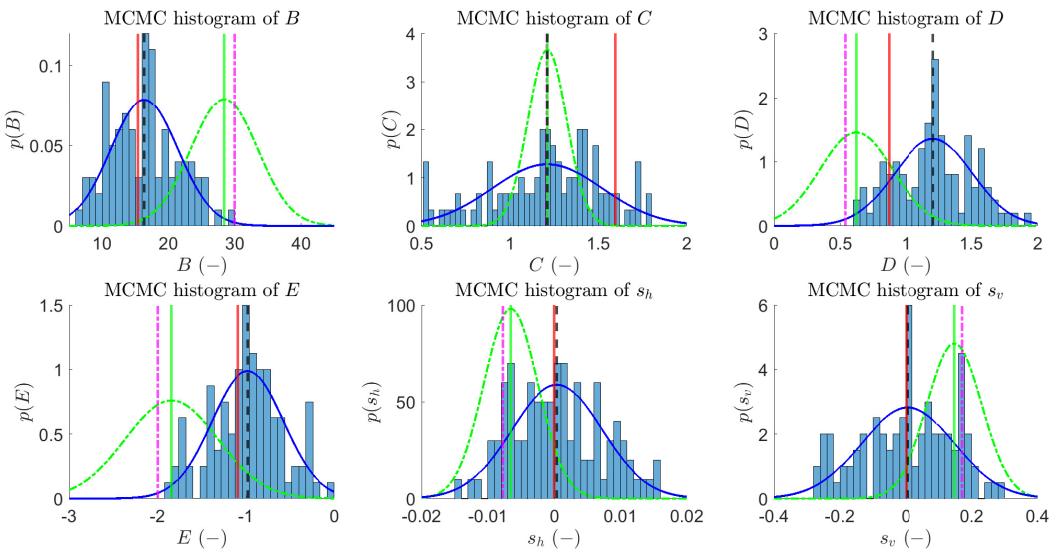

Figure 9: Histograms of the Pacejka's parameters estimated with the MCMC method (for $\mu \leq 0.6$). The red line represents the true value used to generate the friction measurements. The black dashed line indicates the mean of the MCMC estimates. The magenta dash-dot line indicates the minimizer of the loss function. The green line indicates the mean of the ML estimates. The blue line represents a Gaussian pdf fitted to the MCMC estimates. The green line represents a Gaussian pdf fitted to the 10000 ML estimates.

has a length of 30000 samples. In addition, as stated in Algorithm 1, the different chains are initialized with the parameter vector obtained with the ML method. Herein, the ML method is carried out 10000 times similarly to what have been done with the simulated data. Furthermore, the parameter bounds used are still the ones indicated in Table 3.

Remark 4. *In the case treated here, the estimated theoretical covariance matrix obtained with the ML method is*

$$\mathrm{cov}(\hat{\boldsymbol{\theta}}_{ML}) = \begin{bmatrix} 950 & 15.5 & -69.4 & 199 & -1.71 & 69.3 \\ 15.5 & 0.25 & -1.13 & 3.26 & -0.03 & 1.13 \\ -69.4 & -1.13 & 5.01 & -14.5 & 0.13 & -5.06 \\ 199 & 3.26 & -14.5 & 41.8 & -0.36 & 14.5 \\ -1.71 & -0.03 & 0.13 & -0.36 & 0.003 & -0.13 \\ 69.3 & 1.13 & -5.06 & 14.5 & -0.13 & 5.06 \end{bmatrix}, \tag{28}$$

which contains high diagonal elements. As a consequence, this matrix is not suitable for initializing the covariance matrix of the proposal distribution. For this reason, the initial covariance matrix of the proposal distribution is set as the one defined in Eq. (27)*.*

Under such practical conditions, the MCMC based estimation method provides 300 estimates of the friction

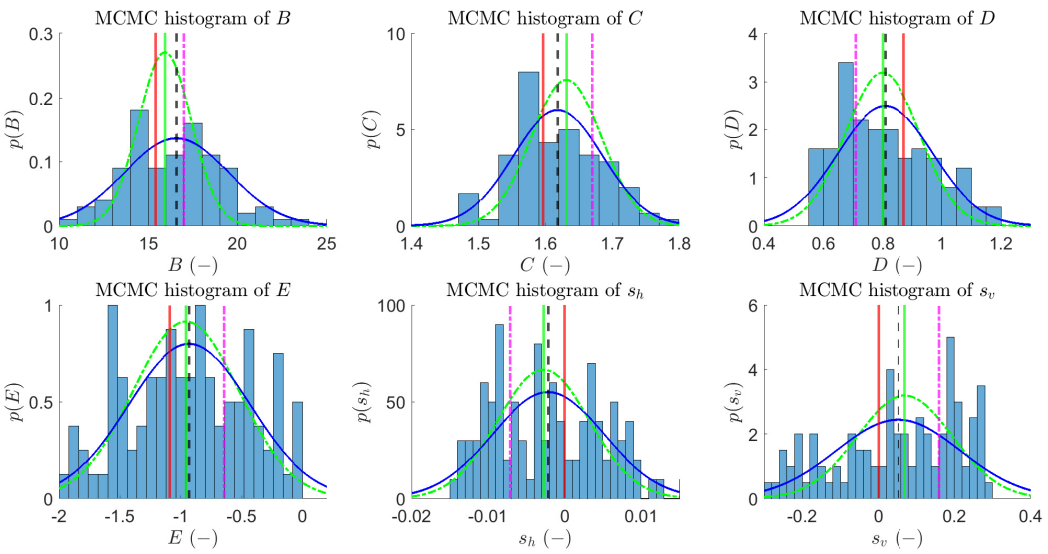

Figure 10: Histograms of the Pacejka's parameters estimated with the MCMC method (all data points selected). The red line represents the true value used to generate the friction measurements. The black dashed indicates the mean of the MCMC estimates. The magenta dash-dot line indicates the minimizer of the loss function. The green line indicates the mean of the ML estimates. The blue line represents a Gaussian pdf fitted to the MCMC estimates. The green line represents a Gaussian pdf fitted to the 10000 ML estimates.

curve represented in grey in Figure 12. The mean of these 300 estimates is plotted in red in Figure 12. In addition, histograms of the grip potentials and their corresponding slip ratio computed with the 300 friction curves are drawn in Figure 13. Finally, Gaussian pdf have been fitted to the estimates obtained with the MCMC based estimation method (see Figure 13). The means and the variances used to fit the pdf correspond to the means and the variances of the 300 estimates. As in the previous section, the ML method have been carried out 10000 times with 10000 different initializations. However, in this case, the resulting grip potential estimates are almost always the same. For this reason, the grip potential obtained with the minimizer of the loss function and the mean of the estimates are approximately equals and thus, are not distinguishable. For the same reason, no ML pdf have been plotted in Figure 13. The friction curve estimated with the ML method is represented in Figure 12. The means and the standard deviations of the different ML and MCMC estimates are summarized in Table 8.

Table 8: ML and MCMC estimates with real data.

Estimation method	μ_{max} mean	μ_{max} standard deviation	$\arg(\mu_{max})$ mean	$\arg(\mu_{max})$ standard deviation
ML	1.223	$2.10e-6$	$3.970e-2$	$3.67e-15$
MCMC	1.222	$2.65e-2$	$4.250e-2$	$4.23e-3$

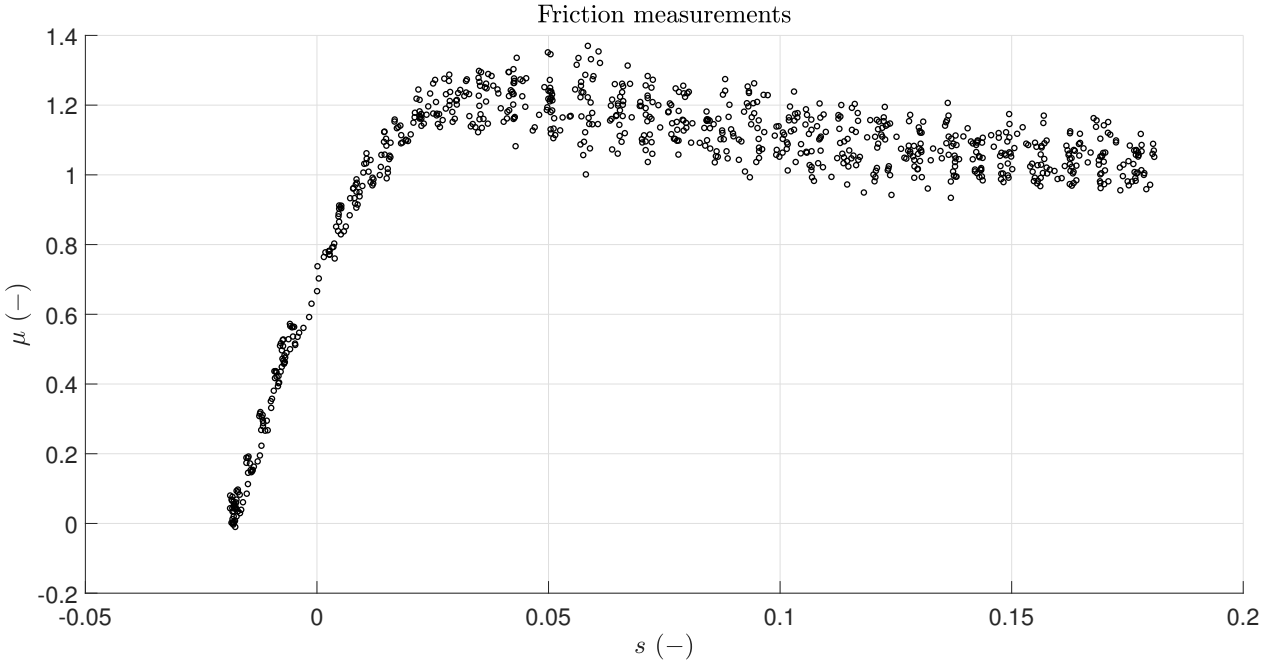

Figure 11: Friction measurements provided by the flat track tire testing machine.

As illustrated in Figure 12, the MCMC estimates match well to the friction measurements. On top of that, the mean of these estimates is almost similar to the one obtained with the ML method. This assertion is reinforced by Table 8 and the histograms in Figure 13 where the friction potential are estimated between 1.15 and 1.3 with a mean equal to 1.222 while the ML value is 1.223. As shown in the second histogram in Figure 13, the slip ratio corresponding to the grip potential estimated with both ML and MCMC methods are close to each other. Indeed, the slip ratio estimated with the MCMC method are situated between 0.03 and 0.055 for a mean value of 0.0425 while the ML value is 0.0397. These results indicate that the MCMC based estimation method works well to estimate the grip potential in the case treated here. More precisely, it delivers mean results similar to the ML method.

Finally note that simulating one chain of 30000 samples has taken around 7.5 seconds. Experiments were conducted with Matlab R2018b on a computer with an Intel core i7 processor running at 2.0 GHz.

Because the ML and the MCMC methods provide an accurate similar estimate of the friction curve when all data points are taken into account, this estimate is now used as a reference. This reference will be used in the following to compare the results obtained with different training sets.

4.2.2. Tests with realistic scenarii

The ML and MCMC estimation methods are now tested with different training sets composed of the data points represented in Figure 11. Each training set is restricted by a different friction limit. The different friction limits start with $\mu = 0.05$ and grow until $\mu = 0.7$ by step of 0.05 for a total of 14 different training

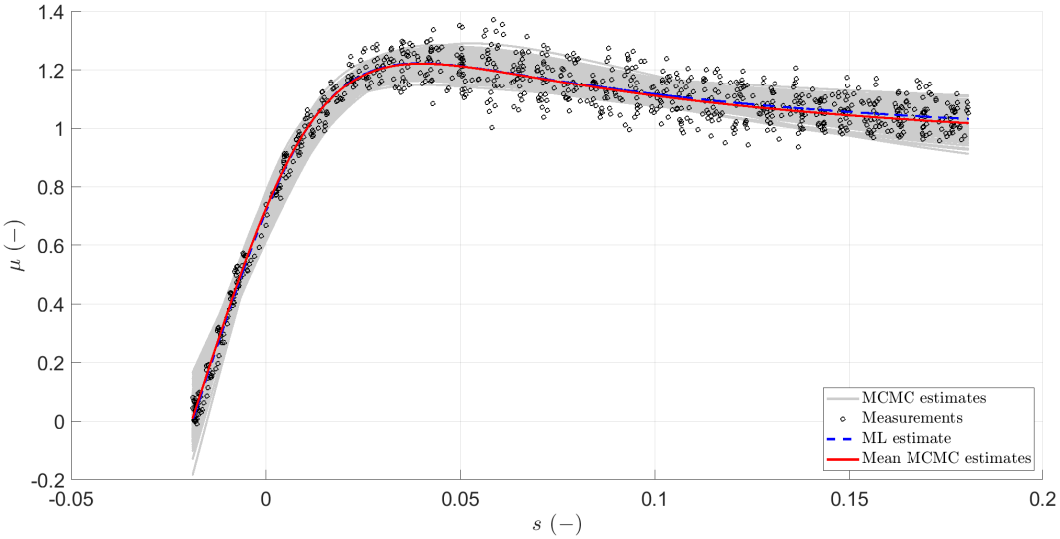

Figure 12: Results of ML and MCMC curve fitting on all the data available. The shadowed area represents the 300 estimates and the red curve the mean of these estimates. The dashed blue line indicates the ML estimate.

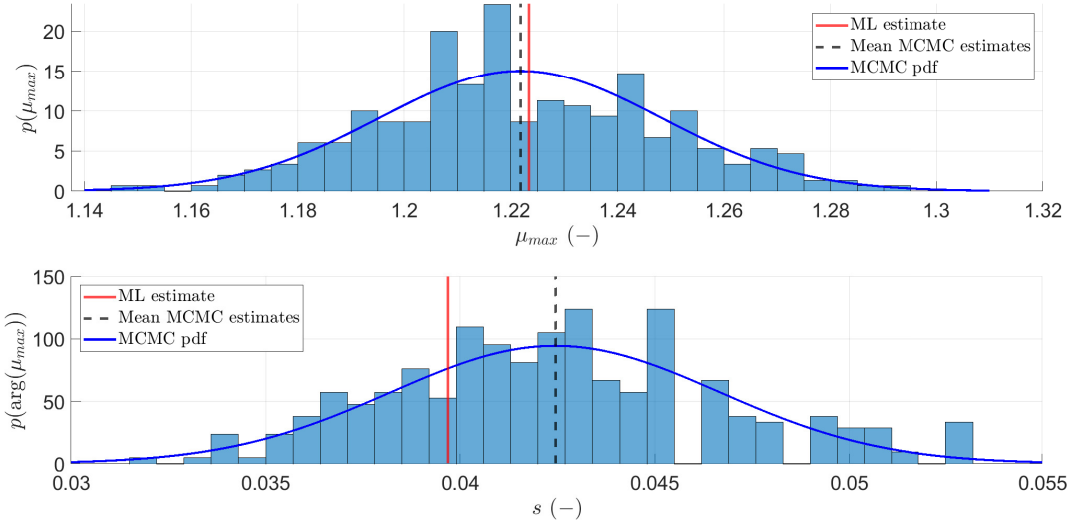

Figure 13: Histograms of grip potential estimates (upper plot) and their corresponding slip ratios (lower plot). The red line represents the values obtained with the ML method. The dashed black vertical line represents the mean of the MCMC estimates. The blue line represents a Gaussian pdf fitted to the MCMC estimates.

sets. Under these practical conditions, the smallest training set contains 24 points and the largest 112 points. Once the training sets are created, it remains to proceed to the initialization of the different methods. For both methods, the parameter bounds are still the ones given in Table 3. As in the previous cases, the ML

method is first performed by picking initials guesses randomly between the parameter bounds. In the different cases treated here, the ML method is performed with 1000 different initial guesses. Furthermore, among all the 1000 ML estimates, the one kept is the parameter vector $\boldsymbol{\theta}_{\mathrm{ML}}$ giving the smallest residual norm. For the MCMC model learning technique, it remains to define the chain numbers and chain lengths. Here, because the training sets are reduced compared to the one considered in the previous case, the estimates obtained with the MCMC method are more likely to vary. For this reason, the number of chains, and thus the estimates, has been set to 1000 with each chain having a length of 100000 samples. Each chain is initialized with the ML estimate $\boldsymbol{\theta}_{\mathrm{ML}}$.

Under such conditions, the MCMC method gives 1000 estimates for each of the 14 training sets. The method performance is assessed by comparing, for the 14 training sets, the relative error between the grip potential of the mean of the MCMC estimates and the grip potential reference. The grip potential reference is the one obtained in the Section *4.2.1* when the ML and the MCMC methods are used with all the available measurements. The same comparison is made with the slip ratio corresponding to the grip potential. Figure 14 shows the evolution of the estimated grip potential with the different estimation methods. Figure 14 also includes the evolution of the relative error of the estimates with the reference value. Figure 15 contains the same type of results about the slip ratio corresponding to the grip potential, *i.e.* the evolution of the estimates and the relative errors. In addition to these curves, Figures 14 and 15 contain a third curve named "MCMC estimate with physical prior" where physical prior is added on MCMC estimates. More precisely, in the situation considered here, we know that the corresponding slip ratio value of the grip potential cannot physically be too high. For this reason, after making the 1000 MCMC estimates, we keep the ones indicating a grip potential with a corresponding slip ratio lower than 0.1 and we consider the mean of these estimates. In this way, the physical prior can be combined with the MCMC based estimation method to improve the final grip potential estimation. Figure 16 indicates the percentage of MCMC estimates rejected after adding physical prior. Figures 17 and 18 show the estimated friction curves obtained in two practical cases. More precisely, when the friction measurements available remain under $\mu < 0.2$ and $\mu < 0.3$, respectively. Besides, Figures 19 and 20 display plots of iterations versus sampled values for each variable in the MCMC chain when added physical prior is considered. The plots are the ones obtained when the used friction measurements remain under $\mu < 0.2$ and $\mu < 0.3$, respectively. Finally, autocorrelation functions (ACF) of two representative Markov chains before and after thinning are plotted in Figures 21-24.

As indicated in Figure 14 and 15, adding physical prior to the MCMC estimates improves the results. Besides, once the training set friction limit is greater than 0.15, the MCMC estimates with physical prior bring more accurate results than the ML method. Indeed, once this friction limit is reached, the MCMC based estimation method provides an estimate of the grip potential with a relative error lower than 20% while the relative error of the estimate obtained with the ML method is almost always greater than 20%. This result is interesting because as mentioned in Section 1, most of the methods used to estimate the grip potential are effective once the grip consumption level is greater than 0.3 [3]. Therefore, estimating the grip

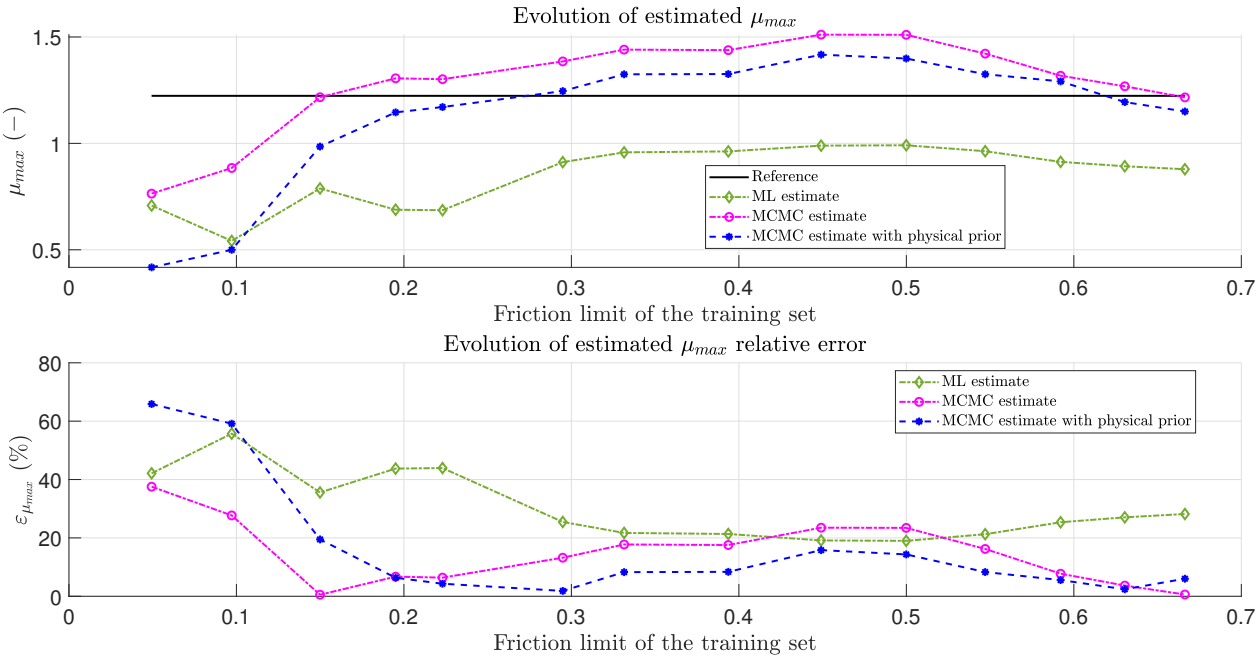

Figure 14: The upper plot represents the evolution of the estimated friction potential obtained with the ML and MCMC methods, respectively. The lower plot represents the evolution of the relative error of the estimated friction potential with the reference value.

potential with a lower friction consumption represents an improvement. Besides, as shown in Figure 16, the percentage of MCMC estimates rejected after adding physical prior decreases with the friction limit. This result suggests that the estimates obtained are more reliable once the friction limit increase. Furthermore, as depicted in Figures 17 and 18, with realistic data sets ($\mu < 0.2$ and $\mu < 0.3$, respectively), the MCMC method estimates friction curves really close to the reference contrary to the ML method. In addition, as shown in Figures 19 and 20, the generated samples stay around mean values which are close to the reference values. Figures 19-20 also indicate that the samples generated with the proposal distribution mix well [34]. More precisely, on the one hand, the samples are not stuck in a small part of the parameter space. On the other hand, the samples are not far from each other. Thus, these traceplots indicate that the generated samples explore the parameter space very well. On another note, according to Figures 21-24, the autocorrelation functions plotted before and after thinning evidence the necessity to remove samples in order to keep chains of uncorrelated samples.

In order to evaluate the method performance more deeply, the histograms of the MCMC estimates of the grip potential and its corresponding slip ratio have been plotted in Figure 25 and 26, respectively.

Figure 25 indicates that the histograms begin to be centered on the reference once the friction limit is equal to 0.2 which corroborates the fact that the method provides satisfactory results from this friction limit measurement value. However, the histogram corresponding to a friction limit of 0.2 in Figure 26 is not clearly centered on the reference value and it does not contain values that emerge from all the estimates obtained.

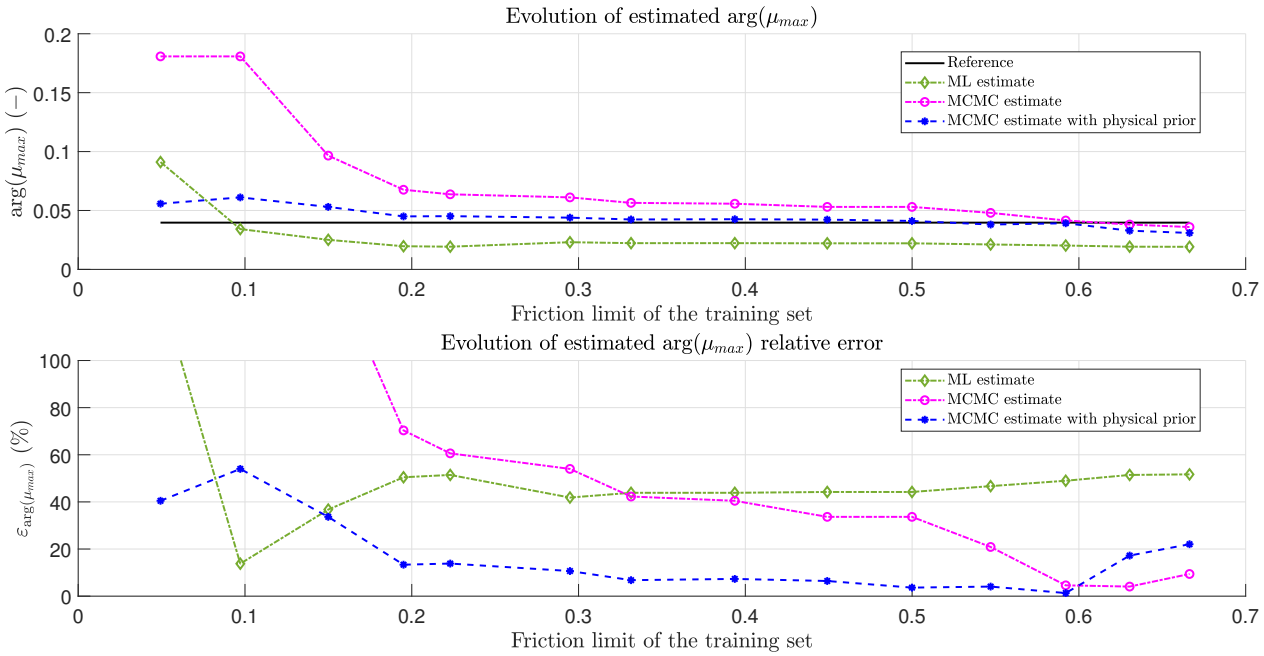

Figure 15: The upper plot represents the evolution of the estimated slip ratio corresponding to the friction potential obtained with the ML and MCMC methods, respectively. The lower plot represents the relative errors with the reference of the estimated slip ratio corresponding to the friction potential.

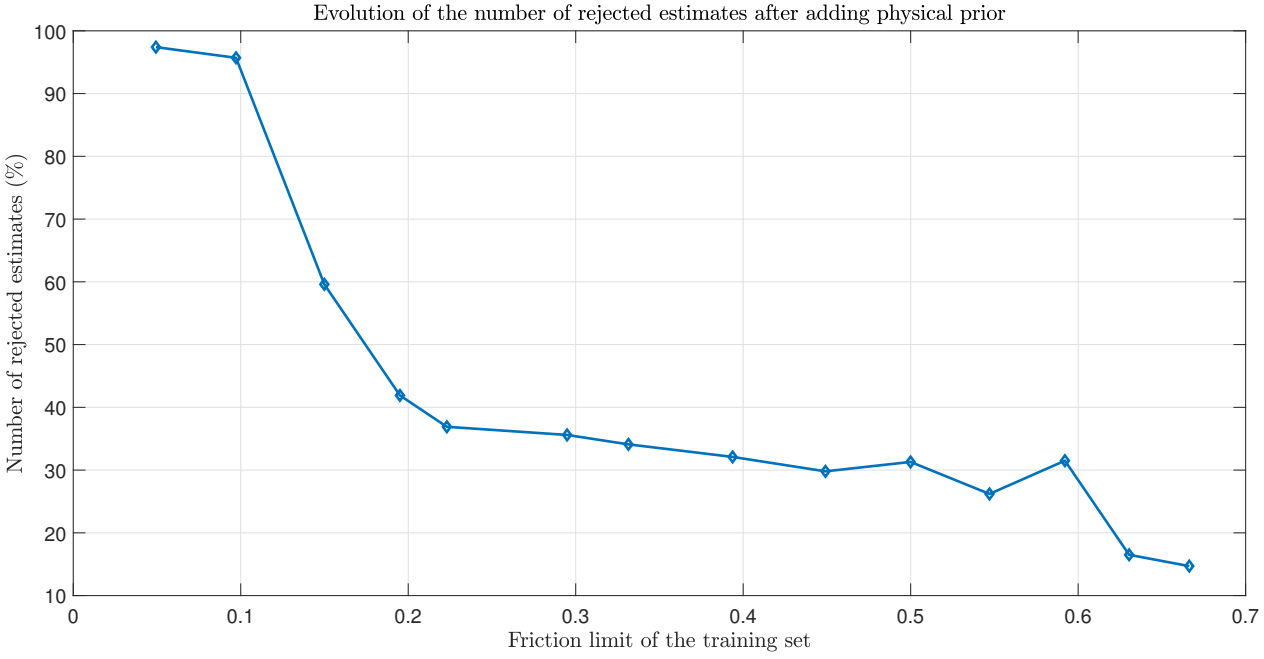

Figure 16: Evolution of the number of MCMC estimates rejected after adding physical prior.

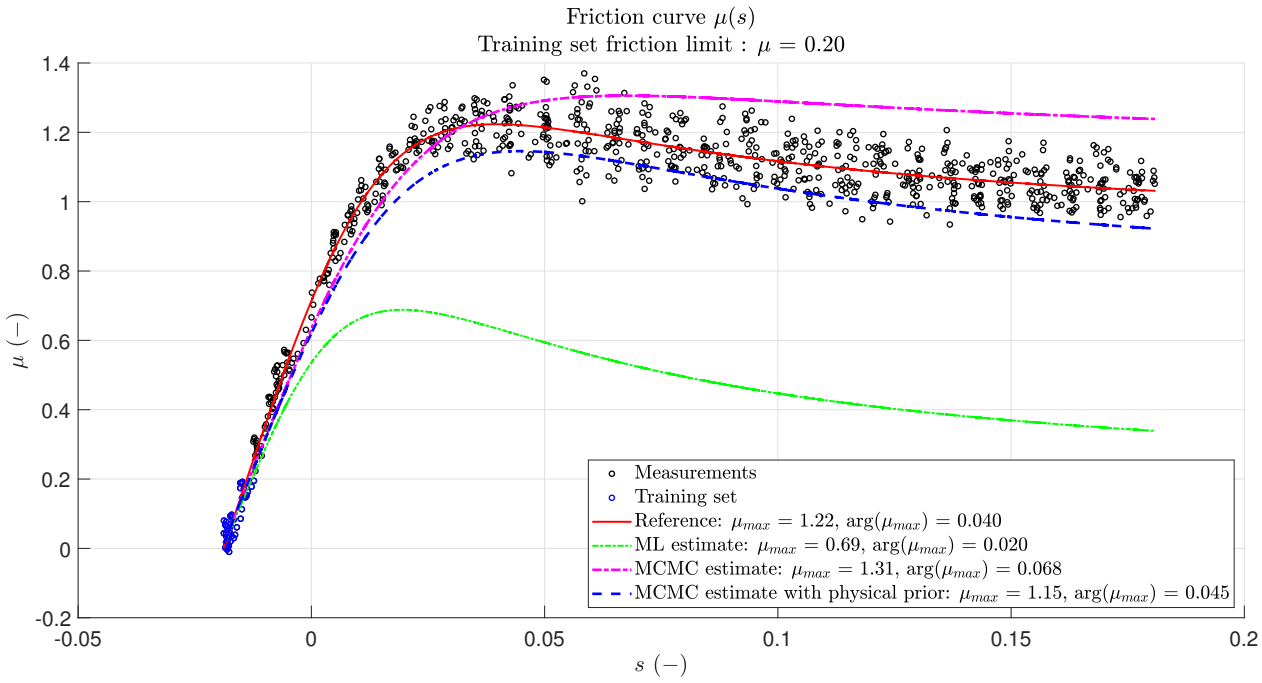

Figure 17: Results of ML and MCMC curve fitting ($\mu < 0.2$). The red line represents the reference friction curve. The dashed-dot green line indicates the ML estimate. The dashed-dot magenta line indicates the MCMC estimate. The dashed blue line indicates the MCMC with physical prior estimate.

Thus, with this friction limit, the grip potential estimate can be accurate but not necessary the associated slip ratio. This situation is not necessarily an issue because we try to estimate the grip potential in priority.

Finally simulating one chain of 100000 samples have taken around 7.5 seconds for the smallest training set and 10 seconds for the largest one.

Characterization of real measurements.

As indicated in the different cases treated in this part, with real data, the MCMC estimates are closer to the reference values than the estimates obtained with the ML method. Looking at the results, we can wonder why the MCMC method works better than the ML method. One reason that could explain these results is the validity of the assumptions made for both methods.

When we described the ML method in Section 3.1, we stated that the stochastic part of the measurements can be modelled with *i.i.d.* Gaussian stochastic components. Now that we have access to real measurements and a reliable estimate of the friction curve (given by ML and MCMC), the residuals can be computed (see Figure 27), then analysed in order to validate the aforementioned assumptions. Two tests are conducted on the residuals, a normality test [47] and an autocorrelation test (ACF)[14]. These tests are carried out on two different training sets in order to ensure that all the measurements have the same statistical properties. The first training set includes the residuals corresponding to friction measurements lower than 0.6. The second

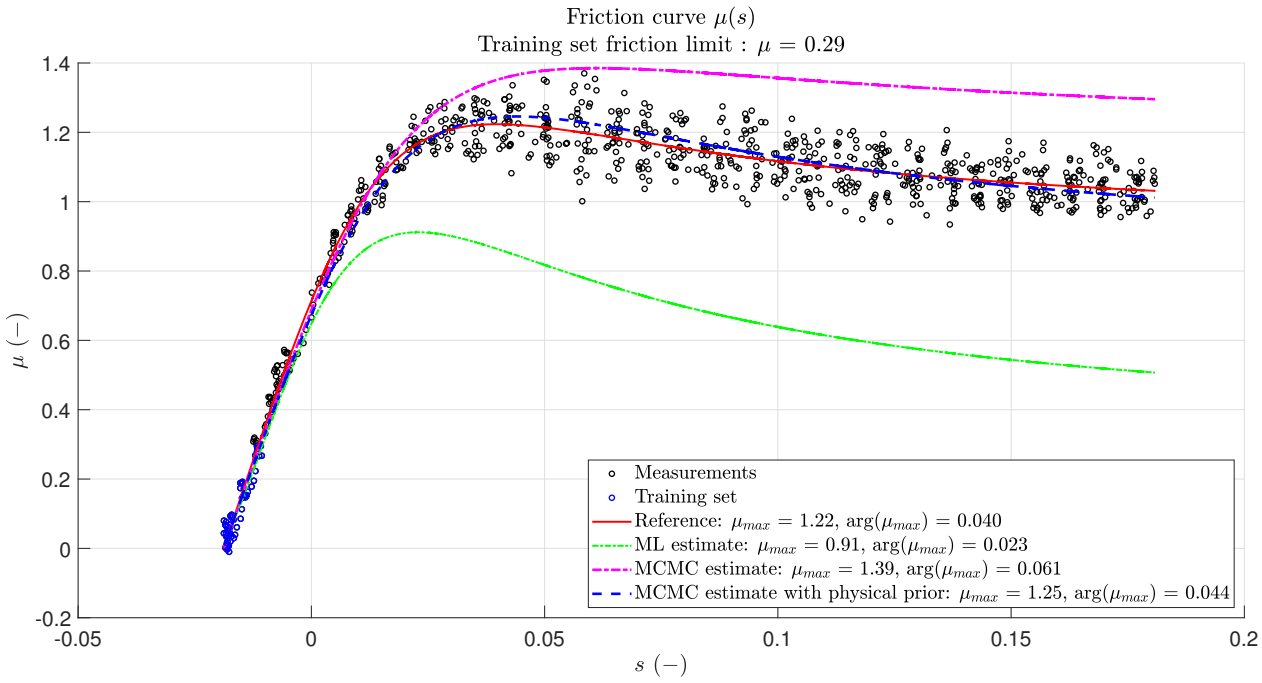

Figure 18: Results of ML and MCMC curve fitting ($\mu < 0.3$). The red line represents the reference friction curve. The dashed-dot green line indicates the ML estimate. The dashed-dot magenta line indicates the MCMC estimate. The dashed blue line indicates the MCMC with physical prior estimate.

data set contains all the residuals.

Firstly, the normality test is performed to verify if the residuals can be model with a Gaussian distribution. The normality test used here is the Kolmogorov–Smirnov test at a significance level of 5% [47]. This one indicates that the null hypothesis cannot be rejected for both residual sets. Besides, this test indicates a $p-$value of 0.8960 when only a part of the residuals are considered and a $p-$value of 0.5339 when all the residuals are selected. Thus, considering the noise normally distributed is a suitable assumption.

Secondly, the ACF test is carried out to verify if the residuals can be considered as independent. As illustrated in Figure 28, it appears that no matter which residual sets is considered, the data points are not *i.i.d.*. Therefore, modelling the stochastic part of the measurements with *i.i.d.* Gaussian stochastic components might not be the most appropriate choice. Furthermore, because the *i.i.d.* assumptions is not valid, it can explained why the ML method provides estimates far from the actual value. The MCMC method seems less sensitive to these assumptions on the measurements. This difference in the sensitivity could explained why the MCMC method provides better estimates than the ML method.

5. Conclusions

In this paper a method combining the Maximum Likelihood approach and an Adaptive Metropolis-Hastings MCMC procedure is applied to determine the tire friction potential. In this method, the ML

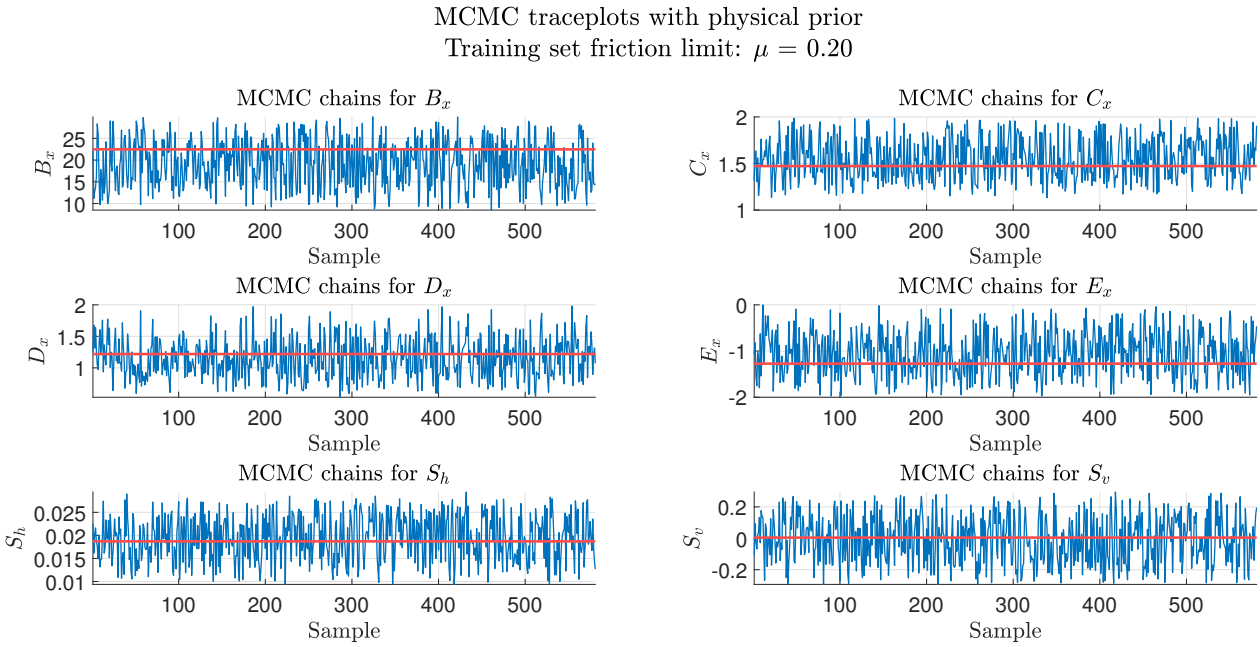

Figure 19: Traceplot of θ_{MCMC} ($\mu < 0.20$) in the case where physical prior is added. The blue curve represents the value of the samples kept. The horizontal red line indicates the reference value.

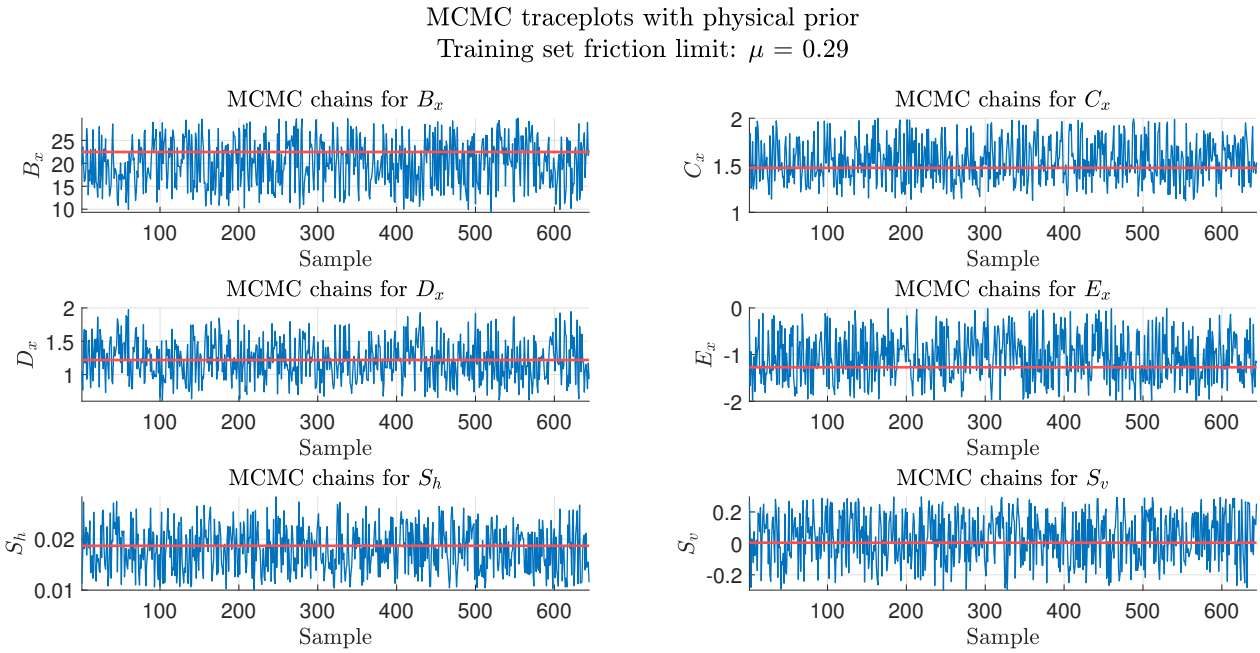

Figure 20: Traceplot of θ_{MCMC} ($\mu < 0.30$) in the case where physical prior is added. The blue curve represents the value of the samples kept. The horizontal red line indicates the reference value.

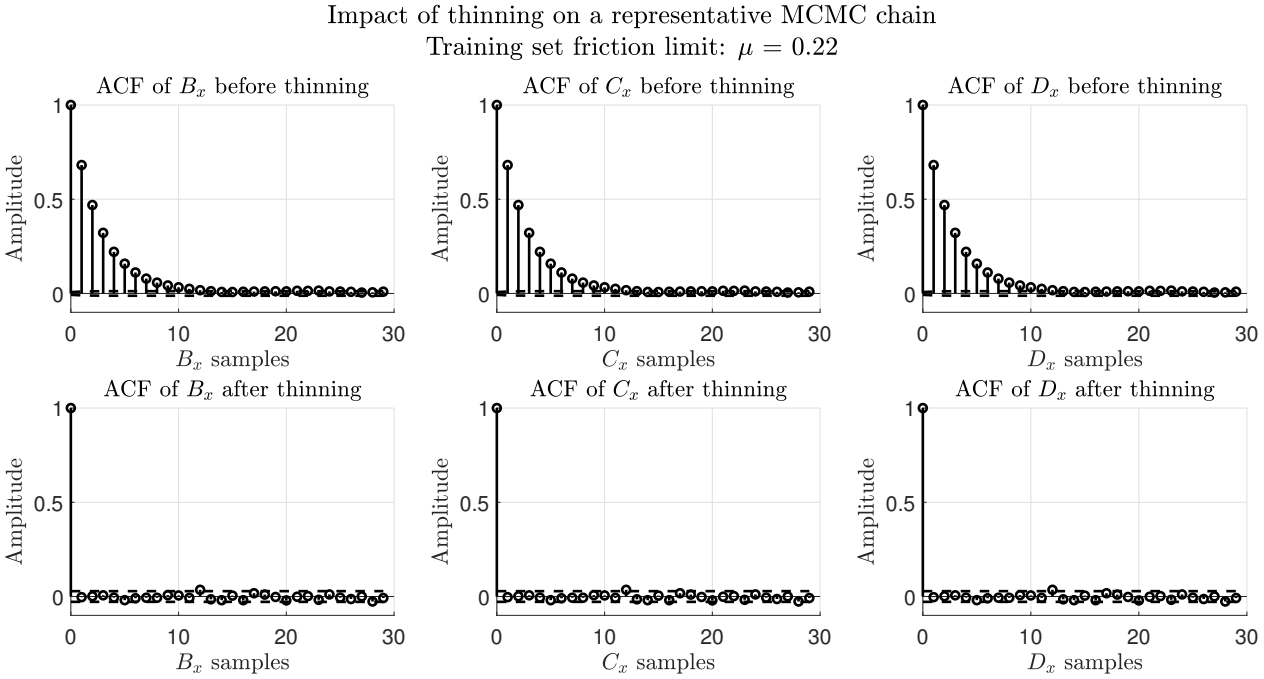

Figure 21: Autocorrelation functions of a Markov chain when the friction measurements are lower than $\mu = 0.25$. The upper figures represent the ACF before thinning. The lower figures illustrate the ACF after thinning. In all figures, the dashed black lines represent the standard error of the ACF with a confidence interval of 95%.

estimates are used to initialize an Adaptive Metropolis-Hastings MCMC algorithm. This method is tested with different training sets coming from both simulated data and real data. The real data is obtained from experiments conducted with a flat track tire testing machine. When data points describing the entire friction curve are selected ($\mu \in [0, 1.2]$), the ML and MCMC methods give equivalent accurate predictions of the Pacejka's model coefficients. However, under standard driving conditions, only friction measurements lower than 0.3 are available. For this reason, the estimation methods are assessed with realistic training sets containing friction measurements under 0.3 only. Under these conditions, the results reveal that the MCMC solution outperforms the classical Maximum Likelihood approach. Indeed, this approach produces accurate estimates as soon as friction measurements reach a value of approximately 0.2. Thus, this result makes the method applicable during standard driving conditions where this range of measurements is accessible.

These results are obtained by assuming that the friction μ is actually measured. However, in practice, the friction data points are not measured but estimated. For this reason, it is necessary to adapt this solution when the friction data is estimated. As suggested in [48], a solution using a Kalman filter is under study.

References

[1] M. Boufadene, A. Rabhi, M. Belkheiri, A. Elhajjaji, Vehicle online parameter estimation using a non-linear adaptive observer, in: Proceedings of the American Control Conference, Boston, Massachusetts,

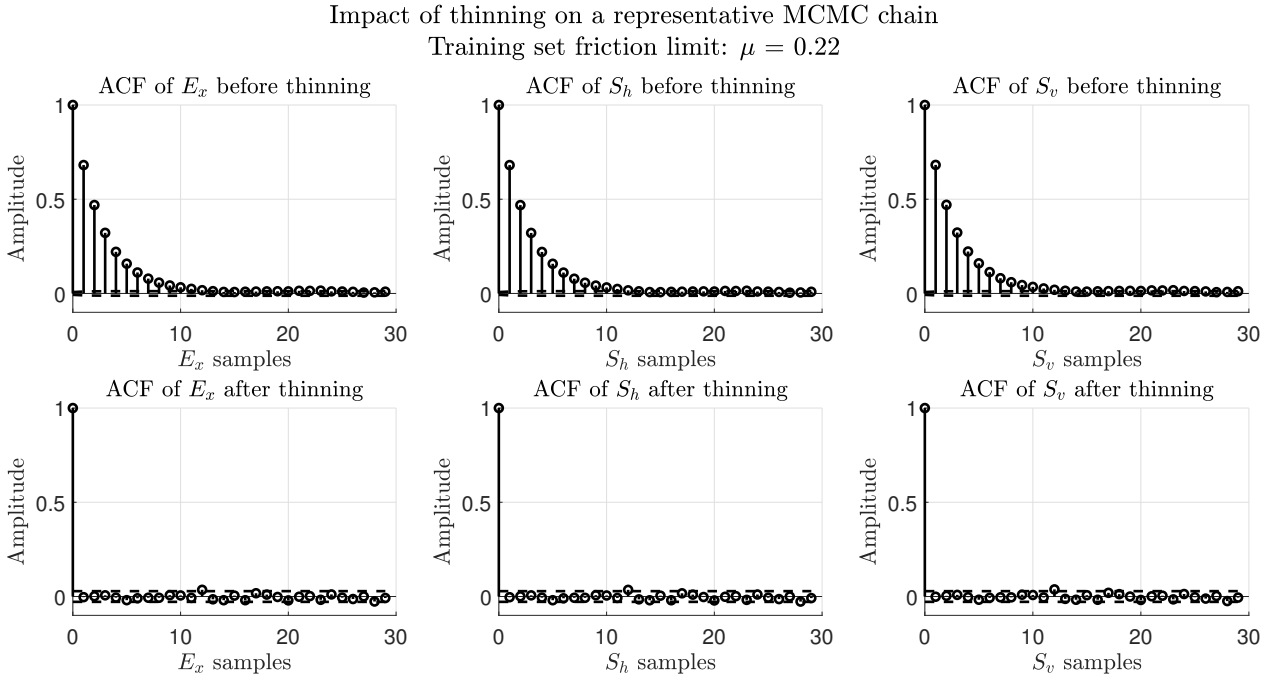

Figure 22: Autocorrelation functions of a Markov chain when the friction measurements are lower than $\mu = 0.25$. The upper figures represent the ACF before thinning. The lower figures illustrate the ACF after thinning. In all figures, the dashed black lines represent the standard error of the ACF with a confidence interval of 95%.

USA, 2016.

[2] D. Burton, A. Delaney, S. Newstead, D. Logan, B. Fildes, Effectiveness of ABS and vehicle stability control systems, Tech. rep., Royal Automobile Club of Victoria Ltd, Victoria, Australia (April 2004).

[3] M. Acosta, S. Kanarachos, M. Blundell, Road friction virtual sensing: A review of estimation techniques with emphasis on low excitation approaches, Applied Sciences 7 (12) (2017) 1230.

[4] J. Piao, M. McDonald, Advanced driver assistance systems from autonomous to cooperative approach, Transport Reviews 28 (5) (2008) 659–684.

[5] K. Berntorp, S. Di Cairano, Tire-stiffness and vehicle-state estimation based on noise-adaptive particle filtering, IEEE Transactions on Control Systems Technology 27 (3) (2019) 1100–1114.

[6] C. Lee, K. Hedrick, K. Yi, Real-time slip-based estimation of maximum tire-road friction coefficient, IEEE/ASME Transactions on Mechatronics 9 (2) (2004) 454–458.

[7] R. Wang, J. Wang, Tire-road friction coefficient and tire cornering stiffness estimation based on longitudinal tire force difference generation, Control Engineering Practice 21 (1) (2013) 65–75.

[8] R. Rajamani, N. Piyabongkarn, J. Lew, K. Yi, G. Phanomchoeng, Tire-road friction-coefficient estimation, IEEE Control Systems Magazine 30 (4) (2010) 54–69.

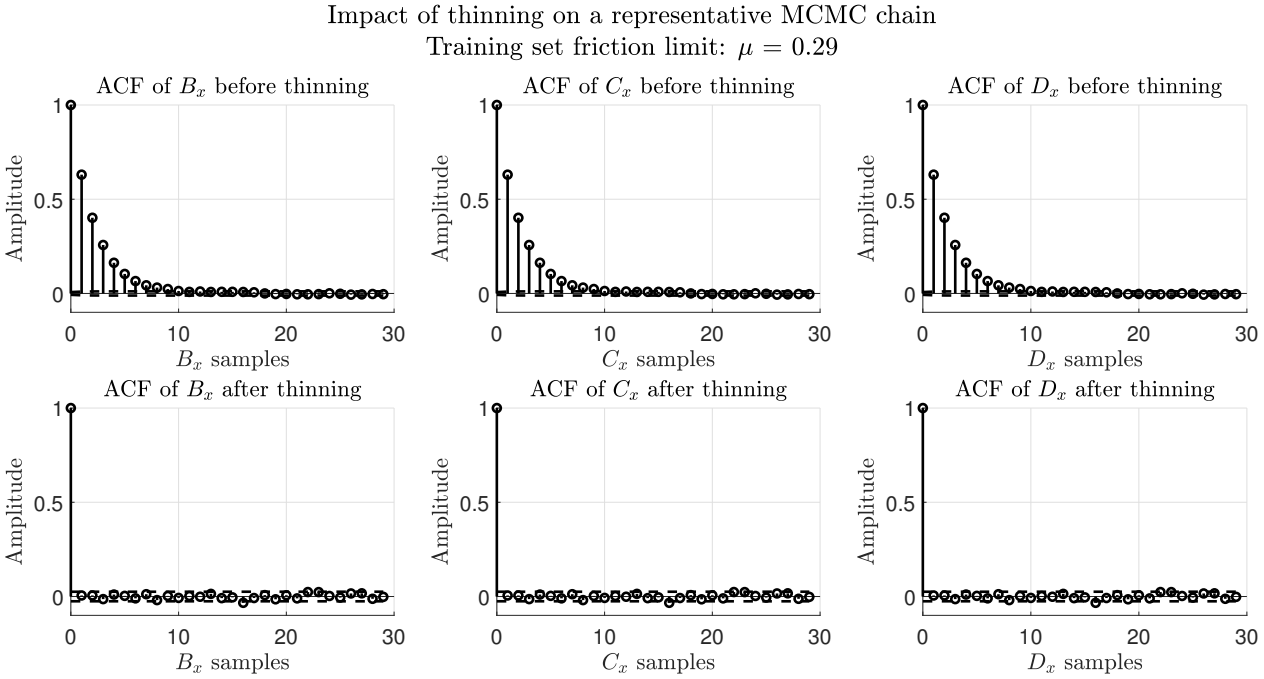

Figure 23: Autocorrelation functions of a Markov chain when the friction measurements are lower than $\mu = 0.30$. The upper figures represent the ACF before thinning. The lower figures illustrate the ACF after thinning. In all figures, the dashed black lines represent the standard error of the ACF with a confidence interval of 95%.

[9] The tyre grip, Tech. rep., Société de Technologie Michelin, Clermont-Ferrand, France (2001).

[10] K. Singh, S. Taheri, Estimation of tire-road friction coefficient and its application in chassis control systems, Systems Science & Control Engineering 3 (1) (2015) 39–61.

[11] S. Khaleghian, A. Emami, S. Taheri, A technical survey on tire-road friction estimation, Friction 5 (2) (2017) 123–146.

[12] K. Singh, M. Arat, S. Taheri, Literature review and fundamental approaches for vehicle and tire state estimation, Vehicle System Dynamics 57 (11) (2019) 1643–1665.

[13] J. Villagra, B. D'Andréa-Novel, M. Fliess, H. Mounier, A diagnosis-based approach for tire-road forces and maximum friction estimation, Control Engineering Practice 19 (2) (2011) 174–184.

[14] S. Rogers, M. Girolami, A first course in machine learning, CRC Press, 2016.

[15] K. Berntorp, Bayesian tire-friction learning by Gaussian-process state-space models, in: Proceedings of the European Control Conference, Naples, Italy, 2019.

[16] M. Acosta, S. Kanarachos, M. Blundell, Virtual tyre force sensors: An overview of tyre model-based and tyre model-less state estimation techniques, Proceedings of the Institution of Mechanical Engineers, Part D: Journal of Automobile Engineering 232 (14) (2018) 1883–1930.

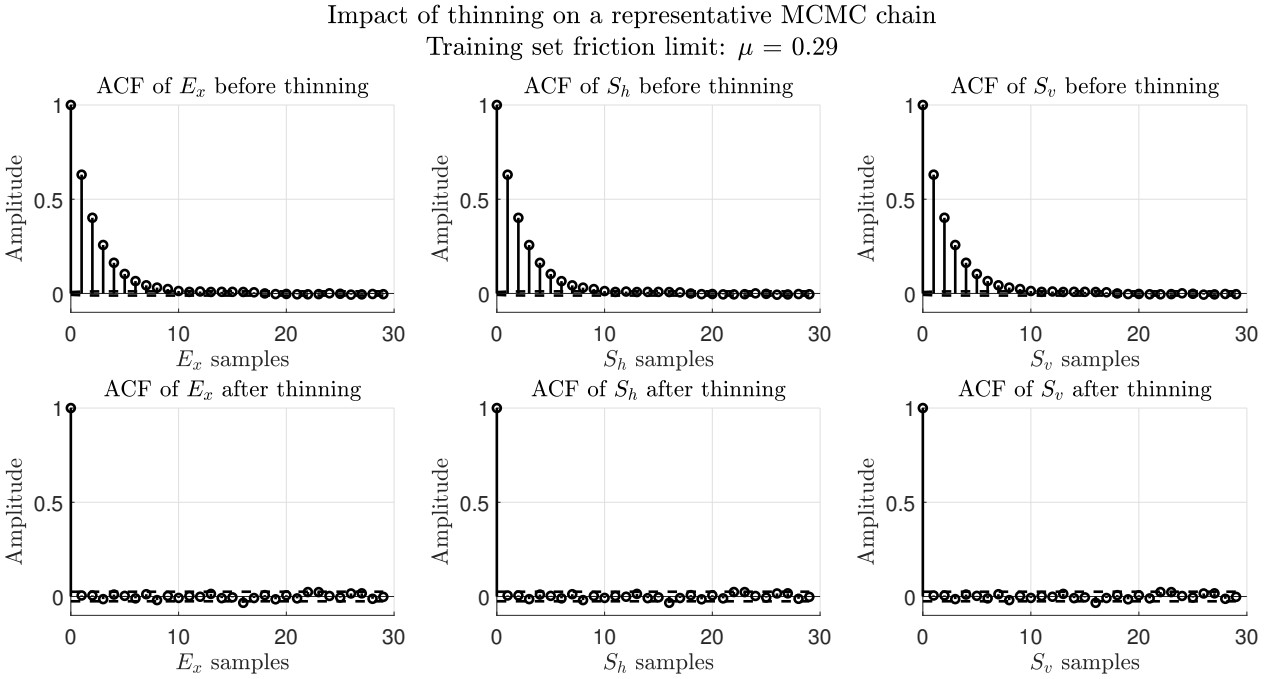

Figure 24: Autocorrelation functions of a Markov chain when the friction measurements are lower than $\mu = 0.30$. The upper figures represent the ACF before thinning. The lower figures illustrate the ACF after thinning. In all figures, the dashed black lines represent the standard error of the ACF with a confidence interval of 95%.

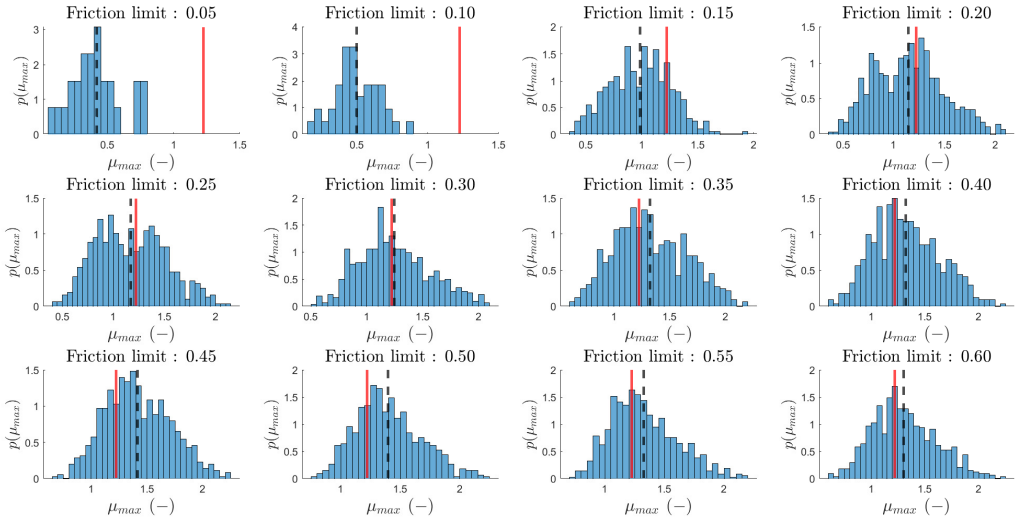

Figure 25: Evolution of the histograms representing the friction potential estimated with the MCMC based estimation method with physical prior. The red line represents the reference value. The dashed black line represents the mean of the MCMC estimates.

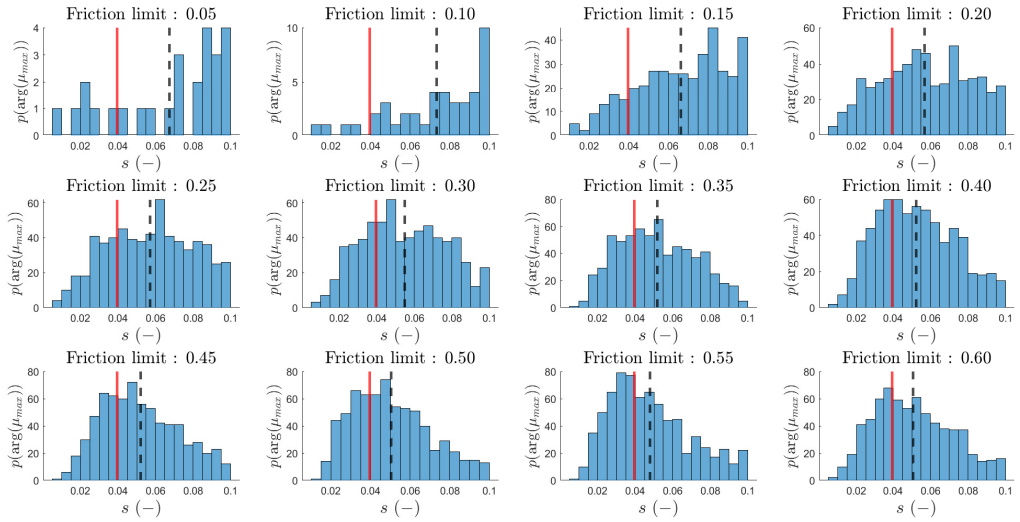

Figure 26: Evolution of the histograms representing the slip ratio corresponding to the friction potential estimated with the MCMC based estimation method with physical prior. The red line represents the reference value. The dashed black line represents the mean of the MCMC estimates.

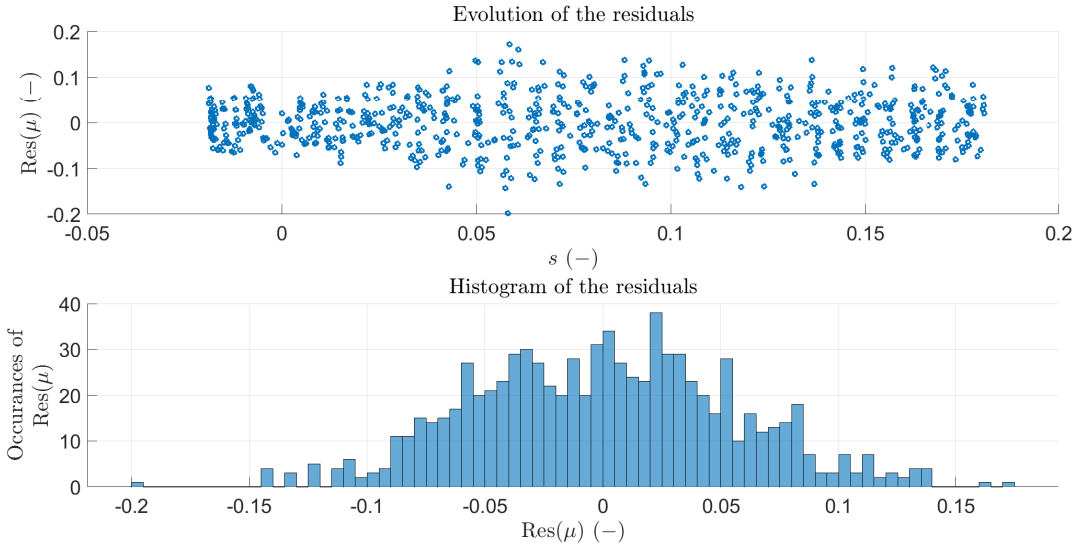

Figure 27: Measurement residuals. The upper plot represents the evolution of the residuals as a function of the slip ratio. The lower plot is an histogram of the residuals.

[17] A. van Zanten, W. Ruf, A. Lutz, Measurement and simulation of transient tire forces, in: Proceedings of the SAE International Congress and Exposition, Detroit, Michigan, USA, 1989.

[18] F. Gustafsson, Slip-based tire-road friction estimation, Automatica 33 (6) (1997) 1087–1099.

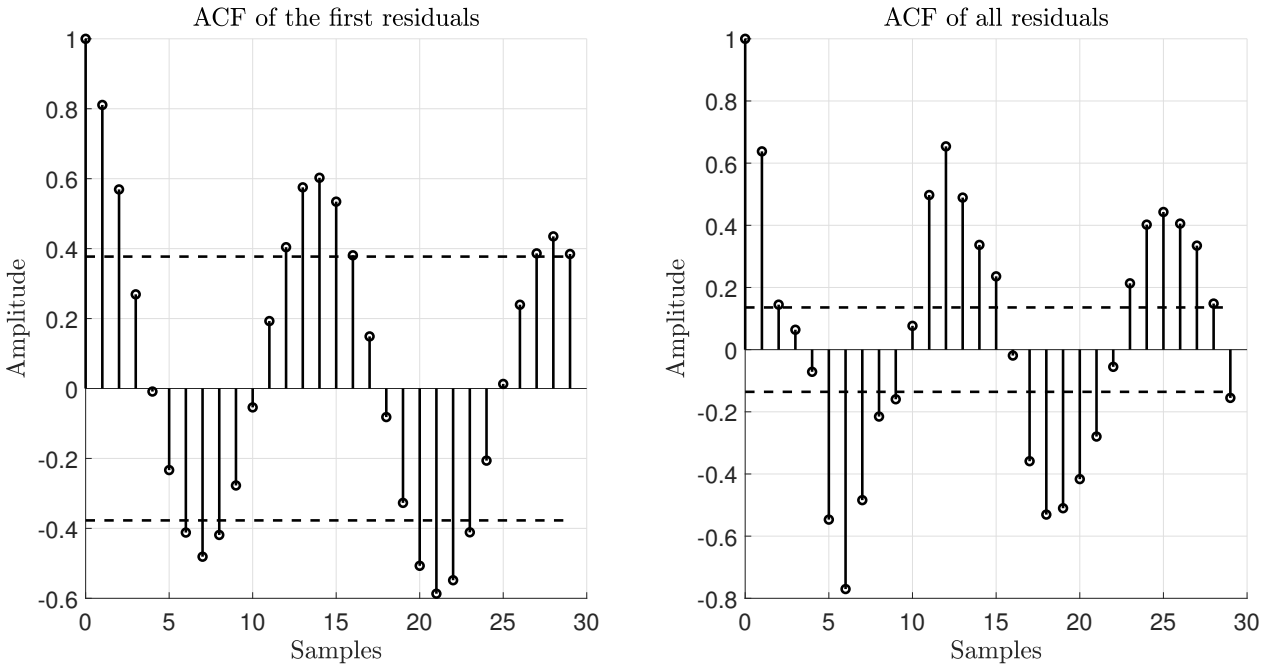

Figure 28: ACF of the residuals. The left figure represents the ACF of the residuals corresponding to the friction measurements lower than 0.6. The right figure represents the ACF of all the residuals. In both figures, the dashed black lines represent the standard error of the ACF with a confidence interval of 95%.

[19] A. Andrieux, P. Vandanjon, R. Lengellé, C. Chabanon, New results on the relation between tyre-road longitudinal stiffness and maximum available grip for motor car, Vehicle System Dynamics 48 (12) (2010) 1511–1533.

[20] D. Luengo, L. Martino, M. Bugallo, V. Elvira, S. Särkkä, A survey of Monte Carlo methods for parameter estimation, EURASIP Journal on Advances in Signal Processing 25 (2020) 1–62.

[21] H. Pacejka, Tire and vehicle dynamics, third edition Edition, Butterworth-Heinemann, 2012.

[22] C. Canudas-de-Wit, P. Tsiotras, E. Velenis, M. Basset, G. Gissinger, Dynamic friction models for road/tire longitudinal interaction, Vehicle System Dynamics 39 (3) (2003) 189–226.

[23] W. DeVinney, Factors affecting tire traction, SAE Transactions 76 (1968) 1649–1656.

[24] R. Rajamani, Vehicle dynamics and control, Springer, 2012.

[25] H. Dugoff, P. Fancher, L. Segel, Tire performance characteristics affecting vehicle response to steering and braking control inputs, Tech. rep., Highway Safety Research Institute, University of Michigan, Ann Arbor, Michigan, USA (August 1969).

[26] C. Canudas-de-Wit, H. Olsson, K. Åström, P. Lischinsky, A new model for control of systems with friction, IEEE Transactions on Automatic Control 40 (3) (1995) 419–425.

[27] H. Szostak, R. Allen, T. J. Rosenthal, Analtical modeling of driver response in crash avoidance maneuvering. volume 2: An interactive tire model for driver/vehicle simulation, Tech. rep., Systems Technology Incorporated, Hawthorne, California, USA (April 1988).

[28] G. Seber, C. Wild, Nonlinear regression, Wiley, 2003.

[29] S. Theodoridis, Machine learning: a Bayesian and optimization perspective, Academic Press, 2015.

[30] A. van den Bos, Parameter estimation for scientists and engineers, Wiley, 2007.

[31] S. Garatti, Assessing the model quality in system identification: the asymptotic theory revisited and application to iterative control, Ph.D. thesis, Politecnico di Milano, Milano, Italy (2004).

[32] C. Robert, G. Casella, Introducing Monte Carlo methods with R, Springer, 2010.

[33] J. Spall, Estimation via Markov Chain Monte Carlo, Control Systems Magazine 23 (2003) 34–45.

[34] C. Andrieu, N. De Freitas, A. Doucet, M. Jordan, An introduction to MCMC for machine learning, Machine Learning 50 (2003) 5–43.

[35] A. Leon-Garcia, Probability, statistics, and random processes for electrical engineering, Pearson, 2008.

[36] J. Nocedal, S. Wright, Numerical optimization, Springer, 2006.

[37] S. Rao, Engineering optimization: theory and practice, Wiley, 2009.

[38] T. Coleman, Y. Li, An interior trust region approach for nonlinear minimization subject to bounds, SIAM Journal on Optimization 6 (1996) 418–445.

[39] S. Kay, Fundamentals of statistical signal processing: estimation theory, Prentice Hall, 1993.

[40] E. Walter, Numerical methods and optimization: A consumer guide, Springer, 2014.

[41] C. Robert, G. Casella, Monte Carlo statistical methods, Springer, 2004.

[42] A. Gelman, J. Carlin, H. Stern, D. Dunson, A. Vehtari, D. Rubin, Bayesian data analysis, CRC Press, 2013.

[43] M. Vihola, Robust adaptive metropolis algorithm with coerced acceptance rate, Statistics and Computing 22 (5) (2012) 997–1008.

[44] S. Särkkä, Bayesian Filtering and Smoothing, Cambridge University Press, 2013.

[45] J. Cabrera, A. Ortiz, A. Simon, F. García, A. Pérez La Blanca, A versatile flat track tire testing machine, Vehicle System Dynamics 40 (4) (2003) 271–284.

[46] J. Olazagoitia, J. Perez, F. Badea, Identification of tire model parameters with artificial neural networks, Applied Sciences 10 (24) (2020) 9110.

[47] H. Thode, Testing for normality, CRC Press, 2002.

[48] L. Ray, Nonlinear tire force estimation and road friction identification: Simulation and experiments, Automatica 33 (10) (1997) 1819–1833.